Disorder and interaction in chiral chains: Majoranas versus complex fermions

J. F. Karcher,[1,2,*] M. Sonner,[1,2,*] and A. D. Mirlin[1,2,3,4]

[1]*Institut für Nanotechnologie, Karlsruhe Institute of Technology, 76021 Karlsruhe, Germany*
[2]*Institut für Theorie der Kondensierten Materie, Karlsruhe Institute of Technology, 76128 Karlsruhe, Germany*
[3]*L. D. Landau Institute for Theoretical Physics RAS, 119334 Moscow, Russia*
[4]*Petersburg Nuclear Physics Institute,188300 St. Petersburg, Russia*

(Received 29 May 2019; revised manuscript received 12 September 2019; published 24 October 2019)

We study the low-energy physics of a chain of Majorana fermions in the presence of interaction and disorder, emphasizing the difference between Majoranas and conventional (complex) fermions. While in the noninteracting limit both models are equivalent (in particular, belong to the same symmetry class BDI and flow towards the same infinite-randomness critical fixed point), their behavior differs drastically once interaction is added. Our density-matrix renormalization group calculations show that the complex-fermion chain remains at the noninteracting fixed point. On the other hand, the Majorana fermion chain experiences a spontaneous symmetry breaking and localizes for repulsive interaction. To explain the instability of the critical Majorana chain with respect to a combined effect of interaction and disorder, we consider interaction as perturbation to the infinite-randomness fixed point and calculate numerically two-wave-function correlation functions that enter interaction matrix elements. The numerical results supported by analytical arguments exhibit a rich structure of critical eigenstate correlations. This allows us to identify a relevant interaction operator that drives the Majorana chain away from the infinite-randomness fixed point. For the case of complex fermions, the interaction is irrelevant.

DOI: 10.1103/PhysRevB.100.134207

I. INTRODUCTION

Topological states of matter represent one of the central directions of the contemporary condensed matter physics [1]. Systems with topological order are usually characterized by a gap in the bulk and "metallic" states at the boundaries. These boundary states are robust against disorder-induced Anderson localization as long as the disorder is not strong enough to close the gap in the bulk [2–5].

One-dimensional (1D) systems with topological phases are considered a potential platform for quantum computing [6–9], as the quantum state is stored nonlocally and cannot be destroyed by local, uncorrelated noise (as long as the noise is not strong enough to close the bulk gap). For noninteracting systems, the symmetry classification by Altland and Zirnbauer [10] combined with the analysis of topologies [11–14], extended also to various spatial symmetries [15,16], has provided a systematic picture of possible topological states. Despite the progress on extending this classification to include weak interactions [17–19], it is still a formidable task to determine which topological phases are present in a given interacting systems. While noninteracting topological phases are robust against disorder-induced localization, this is not always the case for topological states in interacting systems. In particular, in 2D superconductor systems, the combined effect of disorder and interactions has been shown to break entirely the topological protection [20,21]. The underlying mechanism is that disorder renders the interaction relevant in the renormalization-group (RG) sense; see also Refs. [22,23] for related physics. The fact that the interplay of interaction and disorder may crucially affect the physics has been known for a while [24]; recent works show that it is also of central importance for topological states of matter.

In this work, we explore the effect of disorder and interaction on the low energy physics of a chain of Majorana quasiparticles commonly called Kitaev chain [25]. Note that usually one studies the gapped Kitaev chain, with zero-dimensional Majorana bound states at its ends. In this paper, we will pay particular attention to the combined effect of disorder and interaction on a gapless Majorana chain representing a one-dimensional wire with counterpropagating Majoarana modes. The most local interaction one can have in this system is a four-point Majorana interaction [26]. Disorder is introduced by choosing the hopping parameters from a random distribution. This model could potentially be realized by vortex lattices [27–29] in a thin film topological superconductor. In general, chains of parafermions such as Majoranas can also be realized in superconductor-ferromagnet structures along quantum spin Hall edges [30]. Further, the (gapped) Kitaev chain Hamiltonian has been realized as an effective low-energy theory in InGaAs nanowires on top of a superconductor in a magnetic field [31]. A gapless Majorana chain can be realized on the edge of an array of such wires [32]. Other platforms for generating Majorana chains include chains of magnetic atoms on top of a superconductor [33], as well as cold atoms in optical lattices [34]. The phase diagram of a clean interacting Kitaev chain was studied in Ref. [26].

*These authors contributed equally.

We will compare the Majorana model to that of complex fermion hopping on a chain with the chemical potential tuned to zero [35,36]. In spin language, this model is equivalent to the random bond XXZ model. In the absence of interaction, both Majorana and complex-fermion models belong to the symmetry class BDI and are largely equivalent. The only difference between them is that in the case of complex fermions each pair of states related through chiral symmetry represent two independent single body states, while in the case of the Majorana chain each pair represents a single state. However, the situation changes dramatically once one adds interaction. In the case of complex fermions, previous work based on real-space RG analysis showed that weak interactions are irrelevant in the RG sense [35,37] and thus do not change the low-energy properties of the system. This system flows into a peculiar critical infinite-randomness fixed point. For the interacting disordered Majorana chain, the behavior turns out to be very different. We show that interaction drives the system away from the infinite-randomness fixed point, which leads to localization in the case of (even weak) repulsive interaction. The localization of a disordered Majorana chain with moderately strong repulsive interaction was observed previously in Ref. [32]. We further explain why the above two similar models behave so drastically different once interaction is added.

The outline of the paper is as follows. We define the models and review previous results in Sec. II. In Sec. III, we present our numerical results obtained with the density matrix renormalization group [38] (DMRG) code OSMPS [39]. We consider first the clean interacting Majorana chain that we drive out of criticality by staggering in order to explore emerging topological phases. Then we turn to the DMRG study of combined effect of disorder and interaction, both for complex fermions and for Majoranas. In the case of complex fermions, we find that properties of a random chain are not essentially influenced by interaction, in consistency with previous results. On the other hand, we observe that the interacting disordered Majorana chain localizes even for weak repulsive interaction. This localization is accompanied by a spontaneous breaking of symmetry between two topological phases that manifests itself in correlation functions. To shed light on the physical origin of these results, we employ in Secs. IV and V two complementary approaches. Specifically, in Sec. IV, we use momentum-space RG methods to investigate the effect of weak disorder on the interacting clean models. We show that disorder in both models is strongly relevant rendering the clean fixed point unstable. We thus turn to the complementary approach in Sec. V, where we start from an exact treatment of disorder (which drives the system into the infinite-randomness fixed point) and consider interaction as perturbation. By combining the RG treatment of interaction with a numerical study of wave-function correlations at the infinite-randomness fixed point, we identify a relevant operator in the case of the Majorana chain. No such operator exists in the case of the complex fermionic chain in view of the cancellation between Hartree and Fock contributions. This explains why the Majorana fermion chain is unstable with respect to weak interaction, while the complex fermion chain is stable.

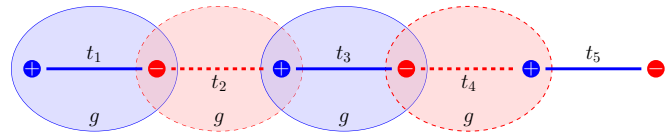

FIG. 1. Sketch of the couplings of the complex-fermion chain with Hamiltonian (2) and $r = 1$. Couplings starting on odd sites are solid, those starting on even sites are dashed. Odd sites have blue color and are labeled by $+$, while even sites have red color and are labeled by $-$. The first few quartic interaction terms involving the sites j and $j+1$ are indicated by blue (odd j) and red (even j) ellipses.

II. MODELS

In this section, we define two 1D models to be considered in this paper: that of complex fermions, Sec. II A, and of Majoranas, Sec. II B. We also briefly review some previous results relevant to this work.

A. Complex fermion chain

We start with a spinless fermionic chain where the chemical potential is tuned to zero,

$$H = \sum_j t_j (c_j^\dagger c_{j+1} + \text{H.c.}). \tag{1}$$

Every hopping term is between an even (e) and an odd (o) site. The Hamiltonian possesses therefore a sublattice symmetry which is represented by the operator $\mathcal{S} = \tau_z$, where τ_z is the Pauli matrix operating on the even-odd subspace. By using the local U(1) gauge freedom, we can always choose the hopping matrix elements t_j to be real. This implies a time-reversal symmetry represented by complex conjugation $\mathcal{T} = \mathcal{K}$ with $\mathcal{T}^2 = 1$. Further, the system possesses in addition the particle-hole symmetry $\mathcal{C}$ expressed by $\mathcal{C} = \mathcal{K}\tau_z$, with $\mathcal{C}^2 = 1$. These symmetries place the model in the BDI symmetry class.

We introduce disorder by making the hopping matrix elements random. This does not change the symmetry classification. The most local interaction that can be added to this model is a two-point nearest-neighbor density-density interaction. To keep the system at half filling, a chemical potential proportional to the interaction strength has to be included. Since we will later see that the sublattice structure of the interaction is important, we generalize the interaction to act on sites separated by a distance r:

$$H = \sum_j t_j (c_j^\dagger c_{j+1} + \text{H.c.}) + g \sum_j p_j p_{j+r}, \tag{2}$$

$$p_j = c_j^\dagger c_j - \frac{1}{2}. \tag{3}$$

The couplings of this model for $r = 1$ are sketched in Fig. 1.

1. Spin representation

Using the Jordan-Wigner transformation, one can map the model (2) onto a random-bond, spin-1/2 XXZ chain:

$$H_{\text{spin}} = \sum_j t_j \left(\sigma_j^x \sigma_{j+1}^x + \sigma_j^y \sigma_{j+1}^y\right) + g \sigma_j^z \sigma_{j+r}^z. \tag{4}$$

The U(1) gauge freedom in the fermionic model corresponds to the spin-rotation symmetry in the XY plane. While the two models (2) and (4) are equivalent, the Jordan-Wigner transformation is nonlocal, and so is the mapping between the correlation functions. The spin representation turns out to be particularly suitable for the DMRG analysis and will be used in this paper.

2. Symmetries and topology

To show that our interaction does not change the symmetry class, we consider the many body generalizations of the above symmetries $\mathcal{T} = \hat{U}_T\mathcal{K}, \mathcal{C} = \hat{U}_C\mathcal{K}, \mathcal{S} = \hat{U}_S$, see Ref. [40]. They can be obtained by defining the action of the symmetry operators on the creation and annihilation operators:

$$\hat{T} c_j \hat{T}^{-1} = (U_T)_{j,i} c_i = c_j, \tag{5}$$

$$\hat{C} c_j \hat{C}^{-1} = (U_C)_{j,i} c_i^\dagger = (-1)^j c_j^\dagger, \tag{6}$$

$$\hat{S} = \hat{T} \cdot \hat{C}. \tag{7}$$

This defines the action of $\hat{T}$, $\hat{C}$, $\hat{S}$ on all operators and states in the Fock space. In this many-body formulation, the time-reversal symmetry $\hat{T}$ and chiral symmetry $\hat{S}$ are represented by antiunitary operators, while the particle-hole symmetry $\hat{C}$ is represented by a unitary operator. In contrast to the single body symmetry operators $\mathcal{C}$ and $\mathcal{S}$, the many body symmetry operators $\hat{C}, \hat{S}, \hat{T}$ all commute with the Hamiltonian.

Let us now analyze the symmetries of the Hamiltonian (2). First, all couplings are real, implying that $\hat{T}$ commutes with H. Second, the term $-1/2$ in Eq. (3), which corresponds to a proper choice of the chemical potential ensures that the model is invariant under $\hat{C}$. Further, the operators $\hat{T}$ and $\hat{C}$ square to unity. The interacting model belongs therefore to the symmetry class BDI. It was shown that 1D interacting systems of complex fermions belonging to this symmetry class (in absence of pairing terms) have a $\mathbb{Z}_4$ topological invariant [19].

3. Clean limit

Let us briefly discuss the clean limit. If all matrix elements t_j are equal, $t_j = t$, and the interaction g is not too strong, the low-energy theory of the XXZ model (4) is the Luttinger liquid. This is a conformal field theory with central charge $c = 1$. For the case of nearest-neighbor interaction, $r = 1$, the corresponding condition is [41] $|g| < t$. For $|g| > t$, the system is gapped.

One can drive the system away from the critical line by introducing a staggering, $t_{2j} = t_\mathrm{e}$ and $t_{2j+1} = t_\mathrm{o}$, with $t_\mathrm{e} \neq t_\mathrm{o}$. This will in general open a gap. More precisely, investigating the RG relevance of the corresponding term in the bosonization language (see analysis in Sec. IV below), we find that the staggering immediately opens a gap for $-1 < g/t < 0.7$, i.e., almost in the whole range of g/t corresponding to a critical theory. The gapped phases with $t_\mathrm{e} > t_\mathrm{o}$ and $t_\mathrm{e} < t_\mathrm{o}$ are topologically distinct. This can be easily seen by observing that in the limit $t_\mathrm{e} \to \infty$, the fermion at the first site decouples from the rest of the chain, thus representing a topological zero mode. This zero mode will persist for $t_\mathrm{e} > t_\mathrm{o}$ (although it will spread over a few sites). In the opposite case, $t_\mathrm{o} \to \infty$, there is no zero mode. The $c = 1$ critical theory (Luttinger liquid) thus represents a boundary between two topologically distinct phases.

4. Noninteracting limit

Consider now a noninteracting system ($g = 0$) but in the presence of disorder, i.e., with random hopping matrix elements t_j. This breaks translational symmetry $j \to j + 1$ for a given realization of disorder. However, if the distributions of even t_{2j} and odd t_{2j+1} matrix elements are the same, the system remains self-dual with respect to the transformation $j \to j + 1$. In spin language, the model corresponds to a disordered XY chain. Analytically, the problem can be treated with a real space RG procedure [35]. At the self-dual point, the system is critical despite an RG flow towards strong disorder. This very peculiar fixed point is termed infinite-randomness fixed point. By considering the scaling of the disorder-averaged entanglement entropy, one can define an effective central charge $c_\mathrm{eff} = \ln 2$ characterizing this critical state [42–44] .

B. Majoranas

To introduce the second model—the one that is which is of the central interest for this work—we start with a 1D chain of spinless fermions of length L with superconducting pairing matrix elements Δ_j, hopping $\tilde{t}_j$, and local chemical potential μ_j. The pairing and hopping are chosen to be real. The Hamiltonian reads

$$H = \sum_{j=1}^{L} \mu_j c_j^\dagger c_j + \tilde{t}_j (c_j^\dagger c_{j+1} + c_{j+1}^\dagger c_j) + \Delta_j (c_j c_{j+1} + c_{j+1}^\dagger c_j^\dagger). \tag{8}$$

Now we rewrite each pair of fermionic creation and annihilation operators in terms of two Hermitian Majorana operators $\gamma_j = \gamma_j^\dagger$:

$$c_j = (\gamma_{2j} + i\gamma_{2j+1})/2, \quad c_j^\dagger = (\gamma_{2j} - i\gamma_{2j+1})/2. \tag{9}$$

The Majorana operators obey the commutation relations

$$\{\gamma_i, \gamma_j\} = 2\delta_{ij}, \quad \gamma_i^2 = 1. \tag{10}$$

Each Majorana operator represents half a degree of freedom. The Hamiltonian becomes now

$$H = \frac{i}{2} \sum_{j=1}^{L} [\mu_j \gamma_{2j}\gamma_{2j+1} + (-\tilde{t}_j + \Delta_j)\gamma_{2j+1}\gamma_{2j+2} + (\tilde{t}_j + \Delta_j)\gamma_{2j}\gamma_{2j+3}]. \tag{11}$$

If the hopping and pairing terms are chosen such that $\tilde{t}_j = -\Delta_j$, this simplifies to

$$H = \sum_{j=1}^{2L} i t_j \gamma_j \gamma_{j+1}, \tag{12}$$

where we have introduced notations $t_{2j} = \mu_j/2$ and $t_{2j+1} = -\tilde{t}_j$. This model is known as Kitaev chain [25].

We now inspect the symmetries of the noninteracting Hamiltonian (8). The pairing terms in Hamiltonian (8)

break the global U(1) symmetry to the parity $\mathbb{Z}_2$. As usual for Bogolyubov-de Gennes models, the Hamiltonian has a particle-hole symmetry $\mathcal{C} = \mathcal{K}$. Since we chose all couplings real, the system has time-reversal symmetry $\mathcal{T} = \tau_z\mathcal{K}$. Both symmetry operators square to unity, thus the model belongs to class BDI. The product of those two symmetries yields the sublattice symmetry $\mathcal{S} = \tau_z$.

Now we include the interaction term. Since $\gamma_n^2 = 1$, the most local interaction term couples four neighboring Majoranas [26]:

$$H = \sum_{j=1}^{2L} it_j\gamma_j\gamma_{j+1} + \sum_{j=1}^{2L} g_j\gamma_j\gamma_{j+1}\gamma_{j+2}\gamma_{j+3}. \tag{13}$$

Below we will allow for randomness in the hopping matrix elements t_j. If the values of the interaction g_j as well as the distribution of hopping matrix elements t_j is the same for even and odd sites, the model is self-dual under translation by one side.

1. Symmetry and topology

The symmetries $\mathcal{T}$, $\mathcal{C}$, and $\mathcal{S}$ can be extended to the many-body setting in analogy with discussion in Sec. II A 2 for the case of complex fermions. In terms of Majorana operators, the symmetries read

$$\hat{T}\gamma_j\hat{T}^{-1} = (-1)^j\gamma_j, \tag{14}$$

$$\hat{C}\gamma_j\hat{C}^{-1} = \gamma_j, \tag{15}$$

$$\hat{S} = \hat{T}\cdot\hat{C}. \tag{16}$$

It is worth mentioning that for Bogolyubov-de Gennes Hamiltonians the particle-hole symmetry is not a true many-body symmetry but rather a constraint related to the Fermi statistics, see discussion in Ref. [45]. This puts our model in interacting symmetry-class BDI with $\mathbb{Z}_8$ topological classification, see Ref. [17].

While the Hamiltonian (13) contains only nearest-neighbor Majorana hopping t_j, any odd-range hopping is, in principle, permitted by symmetry. In particular, as we discuss below, the interaction generates third-nearest-neighbor hopping on the mean-field level. An even-range hopping would couple Majoranas from the same sublattice and break the chiral symmetry and the time-reversal symmetry. Similarly, any interaction term containing an even number of Majorana operators belonging to even sites (and thus an even number of operators from odd sites), is consistent with the $\hat{T}$ and chiral symmetries.

2. Spin representation

The interacting Kitaev chain (13) can be mapped onto a spin-1/2 chain by means of Jordan-Wigner transformation:

$$H = \sum_{j=1}^{L} t_j^{(1)}\sigma_j^x - \sum_{j=1}^{L} t_j^{(2)}\sigma_j^z\sigma_{j+1}^z - \sum_{j=1}^{L} g_j^{(1)}\sigma_j^x\sigma_{j+1}^x - \sum_{j=1}^{L} g_j^{(2)}\sigma_j^z\sigma_{j+2}^z. \tag{17}$$

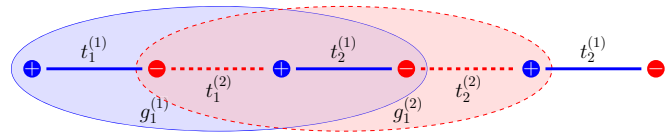

FIG. 2. Sketch of the couplings in the Majorana Hamiltonians (13),(17). Couplings t_{2j} are dashed, t_{2j+1} solid. Odd sites have blue color and are labeled by +, while even sites have red color and are labeled by −. The first two quartic interaction terms with couplings $g_1^{(1)}$ and $g_1^{(2)}$ are indicated by a blue and a red ellipse, respectively. Translation by one site swaps even and odd hopping and interaction terms.

Here, $t_j^{(1)}$ and $t_j^{(2)}$ correspond respectively to odd (t_{2j-1}) and even (t_{2j}) hopping matrix elements of Eq. (13), and similarly for the interaction couplings g. The couplings of this model are sketched in Fig. 2.

It is interesting to note that the odd couplings $g_j^{(1)}$ and $t_j^{(1)}$ couple in the spin language to x components, and the odd couplings $g_j^{(2)}$ and $t_j^{(2)}$ to z components. Translation by one site (even-odd transformation) exchanges $g_j^{(1)} \leftrightarrow g_j^{(2)}$ and $t_j^{(1)} \leftrightarrow t_j^{(2)}$. Models related by this transformation are dual, although this duality is less obvious in the spin representation than in the Majorana representation. We will use the spin representation for the DMRG analysis below.

3. Noninteracting limit

In the noninteracting limit ($g = 0$), the Hamiltonian (17) describes the transverse Ising model. In the clean translational-invariant case [no staggering, $t^{(1)} = t^{(2)}$], the system is critical with a 1D Majorana low-energy theory and central charge $c = 1/2$. In the presence of random hopping, the model is at the infinite-randomness fixed point [37] as noted above in the context of complex fermions in Sec. II A 4. The difference between the two models in the absence of interaction is that two single-particle states of the complex-fermion model correspond to a single state of the Majorana model. As a consequence, the effective central charge at the infinite-randomness fixed point is halved, $c = (\ln 2)/2$.

4. Clean limit

For the case of interacting model with homogenous couplings, $t_j = t$ and $g_j = g$, Rahmani *et al.* [26] have determined the phase diagram.

Strong interaction. The system is gapped for very strong interactions of both signs ($g > 250$ or $g < -2.86$). The translation symmetry gets spontaneously broken, and the transition between the topologically distinct phases is of first order type.

Attractive interaction. There is a critical phase up to very strong interactions $0 < g < 250$. The low-energy theory is a single Majorana mode with central charge $c = 1/2$. This phase is controlled by the same fixed point as the transverse Ising model and therefore dubbed Ising phase.

Weak repulsive interaction. For the case of repulsive interaction ($g < 0$), the Ising phase is stable for sufficiently weak interactions, $g > -0.28$.

Intermediate repulsive interaction. For repulsive interaction of intermediate strength, $-2.86 < g < -0.28$, a phase emerges with coexisting Luttinger-liquid and Majorana modes. Alternatively, one can say that a single Majorana mode of the noninteracting theory is promoted to three Majorana modes, which can be understood already by a mean-field level treatment of the interaction. The central charges in this phase is $c = 3/2$.

III. DMRG RESULTS

It is viable to calculate the groundstate properties of systems with length of the order of a few hundred sites using methods based on matrix-product states (MPS). For these methods, spin models are most convenient. All DMRG calculations in this work have therefore been done on the spin representations, Eqs. (4) and (17), using the software OSMPS [39]. The maximum bond dimension was chosen to be 512, states with weight smaller than 10^{-8} were truncated.

A. Interacting Majorana chain with staggering

As we will later see, disorder drives an interacting Majorana chain into different localized phases if the interaction is repulsive. To obtain an overview over possible localized phases in the Majorana model, we first consider the clean model and drive the system out of criticality by introducing staggering. We calculate the ground state of the clean Majorana chain, Eq. (17) with $t_i^{(1)} = t_1$, $t_i^{(2)} = t_2$, $g_i^{(1)} = g_1$, and $g_i^{(2)} = g_2$, and $L = 96$ spin sites (which corresponds to $2L = 192$ Majorana sites). We choose parameters in such a way that the relation $g_1/t_1 = g_2/t_2$ is maintained; we use a short-hand notation g/t for this ratio. By using DMRG, we explore the range $-4 < g/t < 1$ of the interaction strength, varying the staggering, $0 < t_1/t_2 = g_1/g_2 < \infty$. For the staggering region $0 < t_1/t_2 < 1$, the hopping $t_1 = 1$ is fixed and t_2 is varied, while for staggering above the self-dual line $1 < t_1/t_2 < \infty$, $t_2 = 1$ is fixed and t_1 is varied.

The system with a given value of staggering t_1/t_2 is related to the system with inverse staggering via duality transformation. In the Majorana representation, this transformation corresponds simply to a translation by one lattice site. On the other hand, in the spin language of Eq. (17), the duality transformation is much less trivial (and, in particular, nonlocal).

In the MPS representation, the (von Neumann) entanglement entropy between two subsystems split by a bond is readily available [39,46]. In a critical 1D system of length L with open boundary conditions, the bond entropy scales as a function of bond position x as [47]

$$S(x) = \frac{c}{6} \ln\left(\frac{2L}{\pi} \sin\frac{\pi x}{L}\right) + \gamma, \tag{18}$$

where c is the central charge and γ the topological entanglement entropy. The slope of the dependence of the entanglement entropy on the scaling function entering Eq. (18) can thus be used to extract the central charge of the system. In gapped systems, the entanglement entropy saturates, i.e., $c = 0$.

In order to identify critical lines and regions, the central charge defined according to Eq. (18) is plotted in Fig. 3 via a color map in the parameter plane spanned by the interaction strength g/t and the staggering t_1/t_2. Further, we show in a similar way in Fig. 4 the long-range spin-spin correlation $\langle\sigma^z_{L/4}\sigma^z_{3L/4}\rangle$. This plot helps to differentiate between topologically distinct gapped regions. Figure 5 provides an overview over our results that are discussed in more detail below. In this figure, numbers from 1 to 6 label different regions; the corresponding distance dependencies of spin correlations is shown (with the same labels) in Fig. 6. On the self-dual line, $t_1/t_2 = 1$, the range of interaction strength $-4 < g/t < 1$ can be divided, in agreement with Ref. [26], into three intervals: the $c = 1/2$ Ising phase for attractive and relatively weak repulsive interaction, $g/t > -0.28$, the $c = 3/2$ phase where the Ising sector coexists with a Luttinger liquid sector for

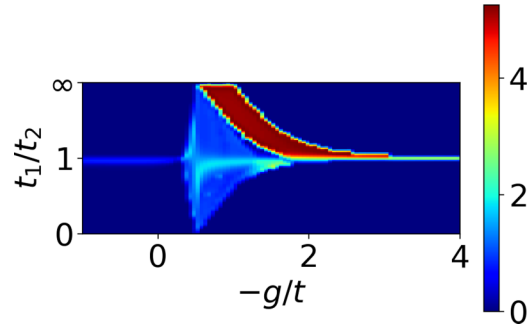

FIG. 3. Central charge c of the clean interacting Majorana chain vs interaction strength $g_1/t_1 = g_2/t_2 \equiv g/t$ and staggering $t_1/t_2 = g_1/g_2$. On the self-dual line (no staggering, i.e., $t_1/t_2 = 1$), the results agree with Ref. [26]: the central charge is $c = 1/2$ for $-g/t \lesssim 0.28$ and is then $c = 3/2$ until the system becomes gapped at strong repulsive interaction, $-g/t > 2.9$. In the Ising phase, the system is gapped everywhere apart from the critical line (i.e., by any staggering $t_1/t_2 \neq 1$). On the other hand, in the Ising + LL phase, adding staggering produces an extend critical region with $c = 1$, see also a schematic phase diagram in Fig. 5. The red patch is a peculiar region where determination of c by means of Eq. (18) breaks down, see Appendix E for more detail. In fact, this phase is gapped (as is also clear by inspecting its dual, $t_1/t_2 \to t_2/t_1$), i.e., the properly defined central charge is zero.

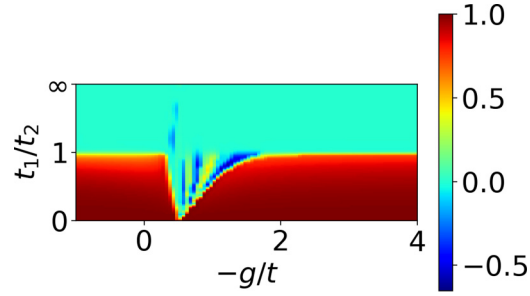

FIG. 4. The $\langle\sigma^z_{24}\sigma^z_{48}\rangle$ correlator between spins on the sites $i = 24$ and 48 for the clean interacting Majorana chain as a function of interaction strength $g_1/t_1 = g_2/t_2 \equiv g/t$ and staggering $t_1/t_2 = g_1/g_2$. In the gapped phases (cf. Figs. 3 and 5), the correlator is equal to zero above the self-duality line and to unity below this line, thus helping to distinguish two topologically distinct phases. In the critical region with $c = 1$ around the Ising + LL phase the correlator shows an oscillatory behavior, cf. Fig. 6, right panels.

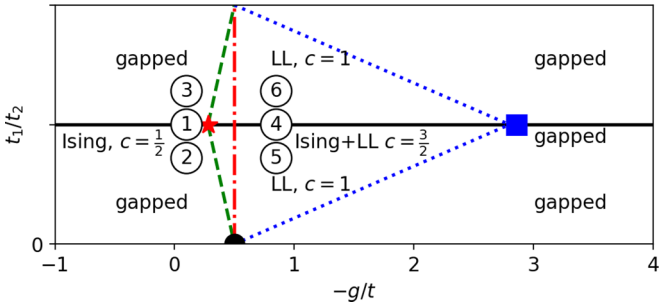

FIG. 5. Schematic phase diagram of the clean interacting Majorana chain in the plane spanned by the interaction strength $g_1/t_1 = g_2/t_2 \equiv g/t$ and the staggering t_1/t_2. The labels from 1 to 6 correspond to the plots of the spin-spin correlator as a function of distance in Fig. 6 which are labeled in the same way. For $-g/t \lesssim 0.28$, the system on the self-dual line ($t_1/t_2 = 1$) is in the Ising phase with central charge $c = 1/2$ (label 1). Introducing staggering yields two topologically distinct gapped phases (labels 2 and 3). At the point $-g/t \approx 0.28$ (marked by a red star), the system undergoes a Lifshitz transition into the Ising + LL phase with $c = 3/2$ (label 4). This Ising + LL phase intersects our projection plane also in the vertical line at $-g/t = 0.5$ (red dashed-dotted line). For intermediate interactions, a not too strong staggering leaves the system gapless but reduces its central charge down to $c = 1$ (Luttinger liquid phases; bounded by green dashed and blue dotted lines, labels 5 and 6). These lines are drawn schematically, their exact form has not been determined. The black dot on the bottom of the diagram ($g_1/g_2 = t_1/t_2 = 0$ and $-g/t = 0.5$) marks the first-order transition in the longitudinal Ising model. The blue square at $-g/t \approx 2.9$ on the self-duality line $t_1/t_2 = 1$ is the point of the transition to a gapped phase. The phase diagram is symmetric with respect to the duality transformation that links points with the same value of g/t and inverse values of t_1/t_2.

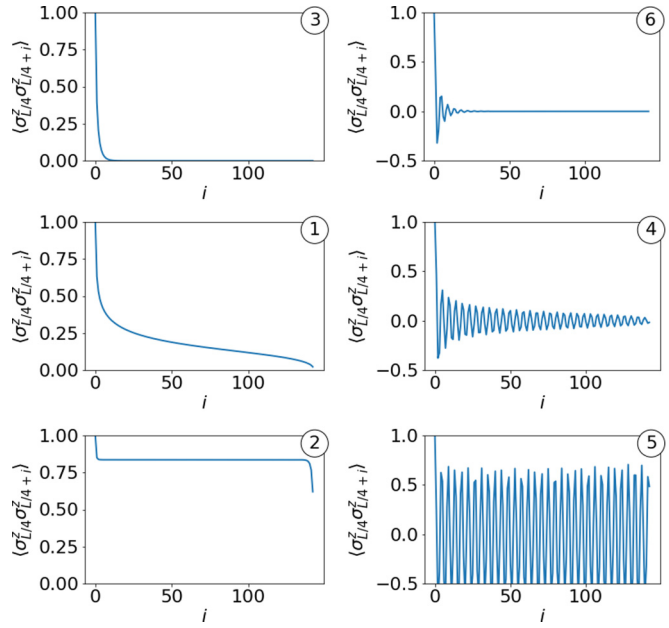

FIG. 6. Spin-spin correlator $\langle\sigma^z_{L/4}\sigma^z_{L/4+i}\rangle$ for the clean Majorana chain in spin formulation, Eq. (17), at weak repulsive interaction $g/t = -0.10$ (left) and medium repulsive interaction $g/t = -0.85$ with no staggering, $t_1/t_2 = 1$ (middle), and staggering $t_1/t_2 = 1.39$ (top) and 0.72 (bottom). The labels from 1 to 6 correspond to those in Fig. 5. The system size is $L = 190$, in the indices $L/4$ denotes the integer part $[190/4] = 47$. In the case of weak repulsive interaction, the correlator is strictly positive, while in the case of medium repulsive interaction, the correlator oscillates as a function of distance and can take on negative values. On the self-dual line (middle), both correlators decay slowly (presumably algebraically) to zero. Above the self-dual line the correlators decay in both regimes quickly (presumably exponentially) to zero. Below the self-dual line, the correlator becomes constant for weak repulsive interaction and oscillates with a constant amplitude for medium repulsive interaction. The drop of the correlator in the bottom left panel (with label 2) near $i = 3L/4$ (i.e., at the right end of the curve) is a boundary effect.

repulsive interaction in the interval $-0.28 > g/t > -2.9$, and a gapped phase for even stronger repulsive interaction, $g/t < -2.9$. This distinction remains useful also for understanding of phases in the presence of staggering, as discussed below.

1. Attractive and weak repulsive interaction

In the absence of staggering, $t_1/t_2 = 1$, the system remains in the noninteracting Ising phase for attractive interaction and for repulsive interaction, $-g/t < 0.28$, as was found in Ref. [26]. Indeed, we observe in Fig. 3 that on the self-dual line the system is critical with a central charge of $1/2$ at this range of interactions. At finite staggering the system is gapped, with two topologically distinct phases (labeled 2 and 3 in Fig. 5) that can be distinguished by the behavior of the spin-spin correlator. For staggering $t_1/t_2 = g_1/g_2 > 1$, which corresponds to the topologically trivial phase in the fermionic picture, it decays quickly with distance, see Fig. 4 and the top left panel of Fig. 6. On the other hand, in the symmetry-broken phase in the spin language, $t_1/t_2 = g_1/g_2 < 1$ (which is topologically nontrivial in the fermion language), the correlator saturates at a constant value of order unity at large distance, Fig. 4 and the bottom left panel of Fig. 6. On the critical line $t_1/t_2 = g_1/g_2 = 1$, the correlator decays slowly (algebraically), as expected, see the middle left panel of Fig. 6.

2. Intermediate repulsive interaction

For stronger repulsive interaction $-0.28 < g < -2.9$, the clean system without staggering exhibits a Luttinger liquid sector in addition to the Ising sector as has been already pointed out in Sec. II B 4. In this paper, we will call this phase "Ising + LL" phase, where "LL" stands for "Luttinger liquid." In Ref. [26], this phase is called the "floating" phase, in analogy to a similar phase in the anisotropic next-nearest-neighbor Ising model. It is characterized by a central charge of $c = 3/2$. Our numerical data in Fig. 3 confirm this behavior.

As Fig. 3 demonstrates, the staggering does not immediately lead to a gapped system in this interaction range. Instead, there is an extended region of finite staggering with a central charge of $c = 1$ around the no-staggering line. This can be understood as a result of the Luttinger-liquid sector being stable to weak staggering, with the Ising sector becoming gapped. An argument based on RG analysis is given in Sec. IV. More precisely, there are two such phases with $c = 1$, labeled 5 and 6 in Fig. 5, which are separated by the line with $c = 3/2$ (label 4).

In these extended critical regions, the spin-spin correlator is an oscillating function of distance, as detailed in Fig. 6. The oscillation decay above the no-staggering line (label 6, top right panel), while their amplitude remains constant below this line (label 5, bottom right panel). On the line without staggering, the oscillations decay very slowly (label 4, middle right panel). The nondecaying oscillation in the extended critical region below the self-dual line are also visible in Fig. 4.

At extreme staggering $t_1/t_2 = 0$, the model reduces to the longitudinal Ising model. This model exhibits a first-order transition at the point $g/t = 0.5$. The critical region with central charge $c = 1$ is separated from the gapped region of the Ising phase by a line connecting this point ($g/t = 0.5$ and $t_1/t_2 = g_1/g_2 = 0$; marked by a black dot in Fig. 5) with the point of the Lifshitz transition on the critical line ($g/t \approx -0.28$ and $t_1/t_2 = g_1/g_2 = 1$; marked by a red star in Fig. 5). Additionally, there is a vertical critical line (red) connecting the black dot to its dual. This line is also clearly visible in the picture of the central charge, Fig. 3, as it has a central charge of $c = 3/2$.

At variance with the horizontal $c = 3/2$ line that is determined by the condition of no staggering, the vertical $c = 3/2$ line is not fixed by any simple symmetry. We have thus performed additional checks to verify its position. First, in order to exclude finite-size effects, we have considered twice larger systems ($L = 192$) in this part of the phase diagram. The results demonstrated that neither the obtained value $c = 3/2$ nor the position of the line change with L. This implies that the vertical $c = 3/2$ line is indeed a property of the system in the thermodynamic limit. Second, we have looked more carefully at the precise location of the line and found that it is not exactly at $-g/t = 0.5$, although very close to it. As an example, we find that the $c = 3/2$ line crosses the horizontal line $t_1/t_2 = 0.72$ at $-g/t \approx 0.45$. This indicates that the "vertical" $c = 3/2$ line is not exactly straight but rather shows a small deviation from the line $-g/t = 0.5$.

Analogous to the horizontal (no-staggering) critical line, the value $c = 3/2$ can be understood as a superposition of a Luttinger liquid ($c = 1$) and a Majorana mode ($c = 1/2$) due to a topological phase boundary. To shed light on the reason for the emergence of the vertical $c = 3/2$ line, we have performed a mean-field analysis by generalizing that of Ref. [48] to our problem. In this way, we have approximately mapped an interacting fermionic Hamiltonian to a noninteracting (mean-field) one and obtained the condition for gap closing. This condition yields a two-dimensional surface in the whole (three-dimensional) space of parameters (t_2/t_1, g_1/t_1, and g_2/t_1). The surface can be computed numerically. We observe numerically that this two-dimensional surface intersects the two-dimensional surface determined by the condition $t_1/t_2 = g_1/g_2$ (that is used in our DMRG numerics) on two lines—the horizontal and the vertical ones. The numerically obtained position of the vertical line is close to $-g/t = 0.5$. With the superimposed extended Luttinger liquid phase, we have $c = 3/2$ on these lines. In analogy with the horizontal line, the vertical line corresponds to the gap closing in the Ising sector, which corresponds to a phase boundary between topologically distinct phases.

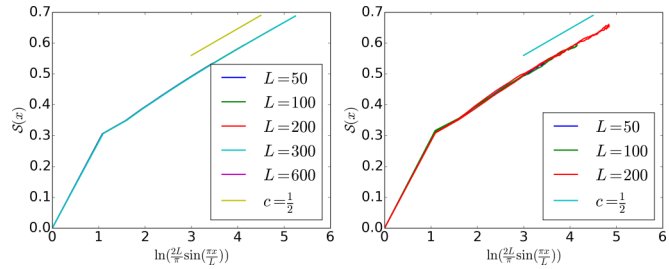

FIG. 7. Entanglement entropy of the clean (left) and disordered (right) Majorana chain with attractive interaction $g = 1$ vs the scaling function Eq. (18) for different system sizes. For the clean system, the central charge is $c = 1/2$ in agreement with Ref. [26]. For the disordered system, the effective central charge is also found to be $c = 1/2$.

Another interesting point is the red patch appearing in the upper plane seemingly violating the duality of the model. This is more than a numerical artifact and has to do with corrections to the scaling form of the entanglement entropy (18) in gapped phases. We refer to Appendix E for a more detailed discussion.

3. Strong repulsive interaction

With increasing strength of repulsive interaction $-g/t$, the extended critical region around the no-staggering line gradually shrinks, see Fig. 3. For sufficiently strong interaction $-g/t > 2.9$ this region vanishes and, moreover, the line of no-staggering becomes gapped.

B. Interacting Majorana chain with disorder

We now introduce disorder in the interacting Majorana chain model by choosing hopping t_j as random independent variables, with a homogeneous distribution over the interval [0.5,1.5]. All hopping matrix elements have now the same distribution, so that there is no staggering.

In general, critical lines can move in phase space as function of disorder strength [49,50]. However, the critical line at no staggering is pinned by self-duality. Therefore it should remain critical in the presence of both disorder and interaction unless spontaneous symmetry breaking takes place, see a more detailed discussion in Sec. III B 2 below.

Since the average value of the hopping matrix elements is unity, the value of the interaction g has now the same meaning as g/t in the analysis of the clean system. We consider three different ranges of interaction strength: (i) attractive interaction $0 < g < 250$, (ii) weak repulsive interaction $0 > g > -0.28$, and (iii) medium repulsive interaction $-0.28 > g > 2.86$. We calculate the effective central charge in these regions of interaction by analyzing the disorder-averaged entanglement entropy via Eq. (18).

1. Attractive interaction

For attractive interaction $0 < g < 250$, the clean system is in the Ising phase [26] with a central charge of 1/2, see Sec. III A 1 and left panel of Fig. 7. On the other hand, the disordered noninteracting system has an effective central charge of $c_{\text{eff}} = (\ln 2)/2 \approx 0.35$ as was found in Ref. [43]. Our numerics confirms this value.

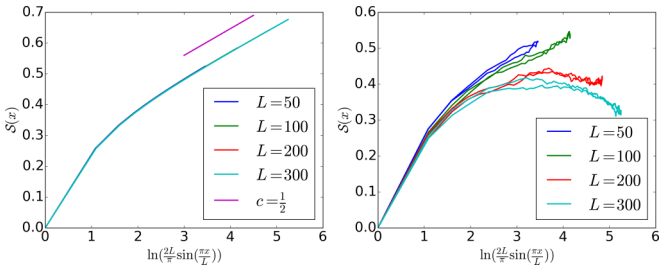

FIG. 8. Entanglement entropy of the clean (left) and disordered (right) Majorana chain with weak repulsive interaction $g = -0.1$ vs the scaling function Eq. (18) for different system sizes. In the clean system, the central charge stays at $c = 1/2$, while in the disordered case the entanglement entropy saturates indicating localized behavior.

Remarkably, in the presence of both disorder and interaction, the central charge returns to the value of the clean system $c_{\text{eff}} = 1/2$, see Fig. 7 (right panel). For higher attractive interaction, the disorder averaging requires less samples in order to give a smooth function of the entanglement entropy versus scaling function than for lower interaction. This serves as an additional indication that disorder does not play an important role for the Majorana chain with attractive interaction.

2. *Weak repulsive interaction*

The clean system stays critical with $c = 1/2$ for weak repulsive interaction [26], $-0.28 < g < 0$, see Sec. III A 1 and the left panel of Fig. 8. We find that adding disorder leads to localization, see right panel of Fig. 8. This appears to happen for arbitrarily weak repulsive interaction and arbitrarily weak disorder. Due to duality, the critical lines have to be mirror symmetric around the self-dual line with respect to staggering. This holds also when the system is disordered. For this reason, the critical line cannot simply bend away from the self dual line. If the system localizes on the self-dual line, there are therefore two possibilities: (i) the critical line splits up into two lines with equal central charge, leaving a gapped region around the self-dual line or (ii) the critical line terminates, and the transition between the region above and below the self-dual line becomes first order. It is shown in Appendix C by treating the interaction at the mean-field level that the criticality is pinned to the self-dual line for all interaction values and disorder strengths. This excludes the option (i), thus implying that the possibility (ii) is realized.

We thus conclude that, for a disordered system with repulsive interaction, the symmetry gets spontaneously broken, and the system undergoes a first-order transition on the self-dual line. This is also reflected in the distance dependence of the spin correlation function. Specifically, we find that, depending on the disorder configuration, this correlation function shows one of two types of behavior: it either very quickly decays to zero or fluctuates around a value of order unity. This is illustrated in Fig. 9 where the results for two disorder configurations are shown. These two types of behavior correspond to two topologically distinct phases, as is clear from the comparison of two panels of Fig. 9 with the top left and bottom left panels of Fig. 6. In the latter figure, the topologically distinct phases were induced by staggering (in a clean model) breaking explicitly the symmetry with respect to the duality transformation. We now see that adding disorder breaks spontaneously the symmetry of the system on the no-staggering line, placing it into one of the two topologically distinct phases. The transition between these two topological phases becomes thus first order.

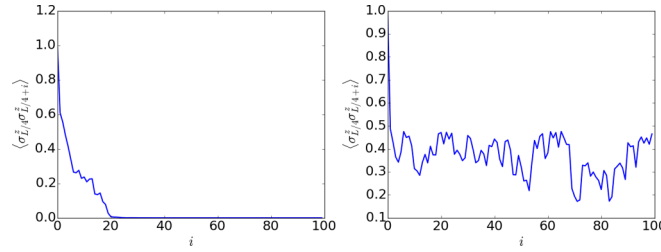

FIG. 9. Spin-spin correlator $\langle\sigma^z_{L/4}\sigma^z_{L/4+i}\rangle$ of the Majorana chain with weak repulsive interaction $g = -0.1$ at length $L = 200$. The two panels represent two different disorder configurations. In the left panel, the correlator decays quickly to zero, which is analogous to the behavior in the presence of staggering $g_1/g_2 = t_1/t_2 > 1$, see top right panel of Fig. 6. In the right panel, the correlation function fluctuates, staying of order $O(1)$. This is similar to the region with staggering $g_1/g_2 = t_1/t_2 < 1$, see bottom right panel of Fig. 6. This behavior reflects the fact that disorder breaks spontaneously the symmetry with respect to duality transformation, placing the system in one of two topological phases.

3. *Medium repulsive interaction*

If the repulsive interaction is in the interval $-2.86 < g < -0.28$, the clean system is in the Ising + LL [26] phase which is characterized by a central charge of $3/2$, see Sec. III A 2 and left panel of Fig. 10. Our results show that, similar to the case of weak repulsive interaction, disorder leads to localized behavior also in this range of interaction, see right panel of Fig. 10. This was also found in Ref. [32].

As in the case of weak repulsive interaction, the spontaneous symmetry breaking by disorder can be visualized by inspecting the spin-spin correlation function for individual realizations of disorder. We find again two distinct types of behavior that are illustrated in Fig. 11: oscillations without decay or with a quick decay. The behavior shown in the left panel of Fig. 11 corresponds to that in the clean model in the Ising + LL phase with staggering $g_1/g_2 = t_1/t_2 < 1$, see

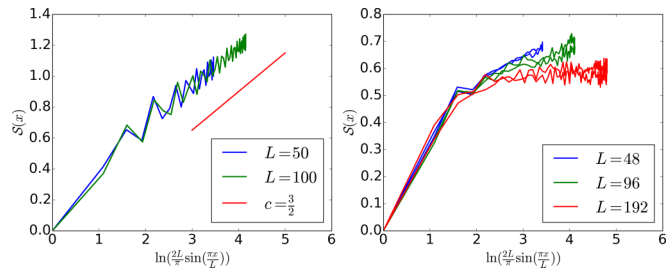

FIG. 10. Entanglement entropy of the clean (left) and disordered (right) Majorana chains with medium repulsive interaction $g = -0.5$ vs the scaling function Eq. (18). The central charge of the clean system is $3/2$ as predicted [26]. On the other hand, the entanglement entropy saturates for the disordered case, implying localization.

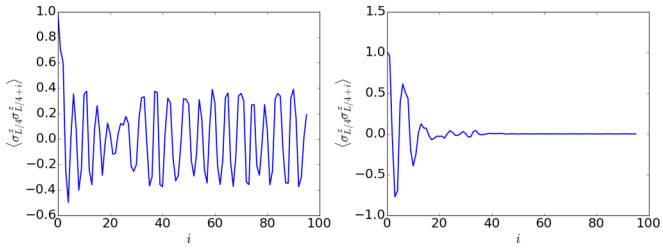

FIG. 11. Spin-spin correlators $\langle \sigma^z_{L/4}\sigma^z_{L/4+i}\rangle$ of the Majorana chain for medium repulsive interaction $g = -0.5$ with length $L = 200$. Two panels show results for two different disorder configurations that lead to vastly different behavior. In the plot for the first disorder configuration, the spin correlator oscillates around zero with an amplitude essentially independent of distance. This behavior is analogous to the one induced by staggering in the region below the self-dual line, see bottom right panel of Fig. 6. For the other disorder configuration, the spin-spin correlator oscillates and quickly drops to zero. This behavior corresponds to the one induced by staggering in the region above the no-staggering line, see top right panel of Fig. 6. The disorder thus breaks spontaneously the symmetry between the two topologically distinct phases. In both phases, the correlator takes negative values for some distances, at variance with the case of weak repulsive interaction, Fig. 9.

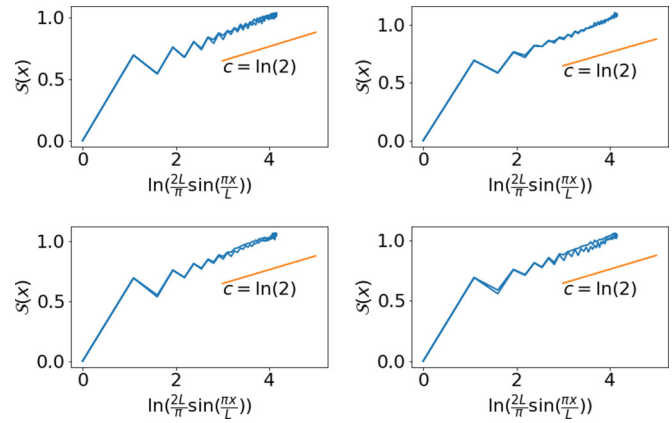

FIG. 12. Disorder-averaged entanglement entropy vs scaling function for an interacting fermionic system with Hamiltonian (2) and parameters $L = 100$, random hoppings t_j drawn from the uniform distribution over [0.5,1.5], as calculated by DMRG. (Left) Attractive interaction $g = 0.1$. (Right) Repulsive interaction $g = -0.1$. The interaction distance is $r = 1$ (top) and 2 (bottom). The scaling of the entanglement entropy corresponds to the value of the central charge $c = \ln 2$, as for a noninteracting system. This indicates that the interaction term is irrelevant in the RG sense.

bottom right panel of Fig. 6, while the behavior shown in the right panel of Fig. 11 corresponds to that in the clean model with staggering $g_1/g_2 = t_1/t_2 > 1$, see top right panel of Fig. 6. Thus the symmetry between the two topological phases gets broken spontaneously by disorder in full analogy with the weak-repulsion regime. A comparison of Figs. 9 and 11 reveals an interesting difference between the weak-repulsion and intermediate-repulsion topological phases. Specifically, in the latter case the correlator shows oscillations around zero, thus changing sign.

C. Disordered fermionic chain

We turn now to the DMRG results for a disordered interacting fermionic chain, Eq. (2). The results for the entanglement entropy are shown in Fig. 12 for the cases of odd ($r = 1$) and even ($r = 2$) interaction distances. We observe that the (sufficiently weak) interaction does not modify the behavior of the disordered system: both for $r = 1$ and 2 the interacting system remains critical and has the central charge $c = \ln 2$ characteristic for the infinite-randomness fixed point. This implies the RG irrelevance of the interaction.

IV. RENORMALIZATION GROUP AROUND THE CLEAN FIXED POINT

Numerical results of Sec. III B for a disordered interacting Majorana chain indicate that in the presence of disorder an interaction of either sign becomes relevant. To get the corresponding analytical insight, one has to consider a model with both interaction and disorder, which is an extremely challenging problem. In this section, we approach this problem by starting from a clean interacting Majorana chain and exploring the effect of weak disorder.

The stability of the clean fixed points of the interacting fermionic and Majorana models can be probed by a weak-disorder momentum-space RG analysis. For this purpose, we consider the low-energy theory in the continuum limit. In the case of the complex fermionic chain, this is a Luttinger liquid (LL) theory. In the Majorana case, it is either a Majorana theory ($c = 1/2$, Ising phase) or a Majorana theory with an additional LL sector ($c = 3/2$, Ising +LL phase), depending on the interaction strength. The density-density parts of the interaction are quadratic in Luttinger theory and renormalize the Luttinger parameter K.

In these continuum theories, disorder appears as a random-mass term. Choosing nonzero average of the mass or a constant nonvanishing mass corresponds to staggering. By including such terms, one can draw conclusions about the stability with respect to staggering, which is another goal of the present section. This should help understanding the appearance of extended gapless phases that were found by DMRG numerical analysis in Sec. III A.

We will show below that at any of the fixed points of the clean Majorana chain (Ising or Ising + LL), the disorder becomes relevant and flows to the strong-coupling regime. This happens also for the complex-fermion fixed point (Luttinger liquid) if the interaction is not too strong. This will lead us to the complementary analysis in Sec. V, where we treat disorder exactly and the interaction as a perturbation.

A. Majorana: $c = 1/2$ fixed point

The continuum decomposition in slow modes $\gamma_{R/L}$ of the lattice Majorana operators γ_j is

$$\gamma_j = \gamma_R + (-1)^j \gamma_L. \tag{19}$$

For Majorana low-energy theory, disorder corresponds to a random-mass term of the form:

$$S_m^{\text{maj}} = \int d\tau dx\, m(x)\gamma_R(\tau, x)\gamma_L(\tau, x). \tag{20}$$

A constant mass $m(x) = m_0$ corresponds to a staggering; it directly opens a gap of size m_0.

The disorder is assumed to be Gaussian white noise with $\langle m(x)m(y)\rangle = D\delta(x-y)$; one can also include a staggering by introducing a nonzero mean $\langle m(x)\rangle = m_0$. Treating the disorder by using the replica trick, one straightforwardly finds that the term generated by disorder has (upon disorder averaging) the scaling dimension 1 and is therefore relevant in the RG sense. This term drives the system away from the clean fixed point. However, this does not necessarily mean that the system becomes gapped. For example, in the noninteracting case (and in the absence of staggering), the system flows to the critical infinite-randomness fixed point [37]. It means, however, that an analysis based on RG around the clean fixed point is insufficient to understand the infrared physics of the problem and suggests a complementary approach as implemented in Sec. V.

Finally it should be noted that no relevant interaction term can be written down in a Majorana low-energy theory. Indeed, the interaction should involve at least four Majorana operators with scaling dimension $1/2$ each and two derivatives with dimension -1. The most relevant term thus has scaling dimension -2 and is strongly irrelevant.

B. Complex fermions: Luttinger liquid ($c = 1$) fixed point

Lattice operators c_j are related to their continuum versions $\psi_{R/L}$ as follows:

$$c_j = i^j \psi_R + (-i)^j \psi_L. \tag{21}$$

In the presence of interaction $g \neq 0$, bosonization has to be employed. Here the following conventions relating the fermionic fields $\psi_{R/L}$ to the bosonic fields ϕ, θ are used:

$$\psi_{R/L} = U_{R/L} \exp(\phi \pm \theta). \tag{22}$$

The Klein factors $U_{R/L}$ are not important in any of the following considerations.

The exact dependence of the Luttinger parameter K on the parameters of the lattice model is known [41]:

$$g/t = -\cos(\pi/2K). \tag{23}$$

Disorder and staggering introduce a mass term of the form:

$$S_m^{\mathrm{LL}} = \int d\tau dx\, m(x)(\psi_R^\dagger(\tau,x)\psi_L(\tau,x) + \mathrm{H.c.}). \tag{24}$$

The scaling dimension of a constant mass term is $2-K$. This means that it is relevant for $K < 2$, which corresponds, in terms of the microscopic parameters, to the interval $-1 < g/t < 0.7$ covering almost the whole range of critical theories, $|g/t| < 1$.

The scaling dimension of the quartic term generated by disorder, as obtained by the replica field-theory approach, is $3-2K$. It depends thus on the Luttinger parameter K whether the disorder is relevant or not. Specifically, for $g/t < 0.5$, the disorder is relevant, while for $0.5 < g/t < 1$ the model remains at the clean fixed point in the presence of weak disorder. We have checked the latter prediction by DMRG, see Fig. 13 for the scaling of the entanglement entropy at strong attractive interaction, $g = 0.8$, and sufficiently weak disorder. We find $c = 1$, as expected for the system at the Luttinger-liquid fixed point. Around the noninteracting limit, i.e., for K sufficiently close to unity, the disorder is strongly relevant, as expected.

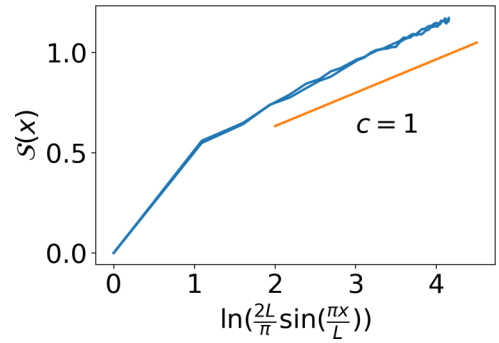

FIG. 13. DMRG results for disorder-averaged entanglement entropy vs scaling function for an interacting fermionic system with Hamiltonian Eq. (2) and parameters $L = 100$, random hoppings t_j drawn from the uniform distribution over [0.5,1.5]. The interaction is attractive and strong, $g = 0.8$, which distinguishes this figure from Fig. 12. The scaling of the entanglement entropy corresponds to the value of the central charge $c = 1$, as for a clean system. The system is at the Luttinger-liquid fixed point with $K > 3/2$ that is stable towards weak disorder, see discussion in Sec. IV B.

We also briefly discuss allowed interaction terms as perturbations to the Luttinger liquid fixed point. They are of three types. First, the density-density interaction is marginal and simply modifies the value of K. Second, terms that are of higher order in ψ or contain gradients are strongly irrelevant. Finally, the staggering yields sine and cosine terms that are relevant in a range of K (in particular, around the weak-interaction point $K = 1$). On the self-dual line, these latter terms are absent.

C. Majorana chain: Ising + Luttinger liquid ($c = 3/2$) fixed point

We turn now to the $c = 3/2$ fixed point of the clean Majorana chain that emerges in a range of medium-strength repulsive interactions, as discussed above. It was suggested in Ref. [26] that, at this fixed point, the low-energy theory consist of Majorana and Luttinger-liquid sectors, see also Secs. II B 4 and III A 2. This can be understood by considering the quadratic form of the action including the third-nearest-neighbor hopping which is generated by a mean-field treatment of the interaction (or, alternatively, under RG flow):

$$H = i\sum_j [t_j \gamma_j \gamma_{j+1} + t' \gamma_j \gamma_{j+3}]. \tag{25}$$

The third-nearest-neighbor hopping term modifies the dispersion such that there are now three Majorana modes, or, equivalently, a fermionic mode emerge in addition to the Majorana mode. The lattice Majorana operator γ_j then has the following low-energy decomposition [26]:

$$\gamma_j = 2\gamma_L + 2(-1)^j \gamma_R + \exp(-ik_0 j)\Psi_L^\dagger + \exp(+i(k_0+\pi)j)\Psi_R^\dagger + \mathrm{H.c.}\,, \tag{26}$$

TABLE I. The RG scaling dimension and relevance range of couplings in the low-energy theory of the Ising+LL phase. Forward scattering is gauged away, see Appendix A. The five remaining (dimensionless) coupling constants corresponding to disorder are labeled y_{k_i}, where k_i refers to the momentum component. The dimensionless interaction strength is denoted by $y' = g' a u^{-1}$, where a is the lattice spacing and u the LL velocity. The clean Ising+LL phase of the Majorana chain is characterized by $K < 1$ and remains stable with respect to coupling between the Ising and LL sectors as long as [26] $\frac{1}{4} < K < 1$.

coupling	dimension	relevant in
y_{k_0}	$2 - \frac{1}{2}(K + K^{-1})$	$0.27 < K < 3.8$
$y_{k_0+\pi}$	$2 - \frac{1}{2}(K + K^{-1})$	$0.27 < K < 3.8$
y_{2k_0}	$3 - 2(K + K^{-1})$	$0 < K < 2$
$y_{2k_0+\pi}$	$3 - 2K$	$K < 1.5$
y_π	$3 - 2K^{-1}$	$0.67 < K$
y'	$1 - K^{-1}$	$1 < K$

where k_0 is the effective Fermi momentum. The interaction $g\gamma_j\gamma_{j+1}\gamma_{j+2}\gamma_{j+3}$ generates now the density-density interaction of the fermions Ψ_R, Ψ_L. To treat this interaction exactly, we employ the bosonization approach. Another interaction term couples the resulting Luttinger liquid to the Majoranas with strength g', see Eq. (A2).

Next, let us discuss the stability with respect to staggering. The kinetic term $\gamma_j\gamma_{j+1}$ has oscillatory components with wave vectors $k_i = 0$, k_0, $k_0 + \pi$, $2k_0$, $2k_0 + \pi$, and π. A constant mass term $m(x) = m$ describing staggering couples to the π component of the kinetic term:

$$S_m = \int d^2r[-8m\gamma_L\gamma_R + 4m\cos k_0 \cos 2\theta]. \qquad (27)$$

The Majoranas are then immediately gapped out. On the other hand, the cosine term in the Luttinger-liquid sector is relevant only for $K > 1/2$. There is therefore a region of the interaction strength where the Luttinger liquid is stable towards staggering. This explains the existence of the extended gapless phase with $c = 1$ observed numerically, see Fig. 3 and the schematic phase diagram in Fig. 5.

Now we analyze the effect of disorder that is treated as a weak perturbation. Combining the oscillatory components of the kinetic term $\gamma_j\gamma_{j+1}$ (with the six wave vectors listed above) with the corresponding Fourier components of the random mass yields nonoscillatory contributions. We get therefore six independent disorder couplings D_{k_i} that coincide at the beginning of the RG flow but renormalize differently. Details on implementation of the RG procedure are presented in Appendix A. In Eq. (A1), the disorder-induced terms in the action (with the replica formalism used to average over disorder) are presented. While the forward scattering D_0 cannot be gauged away straightforwardly, a more detailed calculation shows that it does not change the results presented here.

In Table I, we list the scaling dimensions of the disorder couplings resulting from the corresponding RG equations. They determine the range of K in which the disorder-induced terms are RG-relevant. We observe that at least one of the couplings is relevant for any value of K, i.e., the disorder always drives the system aways from the clean fixed point. In analogy with the conventional Giamarchi-Schulz RG [51], the RG equations for the disorder-induced couplings are complemented by the flow equation for the Luttinger constant K:

$$\frac{\partial K}{\partial \ell} = -\frac{1}{2}\left[K^2 - \frac{(1+K^2)(3-2K)}{2}\right] y_{2k_0+\pi} + \frac{1}{2}\left[1 - \frac{(1+K^2)(3-2/K)}{2}\right] y_\pi . \qquad (28)$$

Here, $y_{2k_0+\pi} = \pi^{-1} D_{2k_0+\pi} a u^{-2}$ and $y_\pi = 16\cos^2 k_0 D_\pi a u^{-2}$ are dimensionless coupling constants for the disorder-induced terms with momentum component k_i in terms of lattice spacing a and Luttinger-liquid velocity u. In Eq. (28), we have kept only the contribution of the couplings $y_{2k_0+\pi}$ and y_π to the renormalization of K. In principle, the other couplings y_{k_i} also contribute to this renormalization; however, they are less relevant for K around unity, so that we have neglected their contributions.

A brief summary of main conclusions that we draw from this RG is as follows. First, the Ising + LL clean fixed point is stable towards interaction. Indeed, this phase is characterized by a repulsive interaction, hence $K < 1$, so that the y' coupling is irrelevant. In fact, a higher order coupling between the LL and Majorana sectors becomes relevant for very strong interaction [26], $K < 1/4$, so that the range of stability in the absence of disorder is $1/4 < K < 1$. Second, over an extended parameter regime, the staggering is irrelevant in agreement with the numerical results of Sec. III A 2, see Fig. 3. Third, and most importantly, the disorder at the Ising + LL fixed point always runs to strong coupling. In other words, this fixed point is unstable with respect to disorder.

The results obtained in Sec. IV demonstrate that the weak-disorder analysis is not sufficient for Majorana chain, both in the $c = 1/2$ and $c = 3/2$ phases of the clean system. The RG relevance of disorder is also supported by the analysis in Appendix C where the exact treatment of disorder is combined with mean-field treatment of the interaction. The disorder is also RG relevant for the complex-fermion chain if the interaction is not too strong. These results motivate us to perform in Sec. V a complementary analysis. We will start there from an exact treatment of disorder and will include interaction as a weak perturbation.

V. STRONG RANDOMNESS FIXED POINT: EIGENFUNCTION STATISTICS AND EFFECT OF INTERACTIONS

In Sec. IV, we have seen that the combined effect of interactions and disorder cannot be understood as a perturbation around the clean interacting fixed point. Specifically, we have established that disorder is strongly relevant at the clean fixed point, thus quickly increasing under RG. We know that, in the absence of interactions, this RG flow leads to the critical infinite-randomness fixed point. It is thus a natural question whether this fixed point is stable or not with respect to interactions. This question is addressed in the present section. Our analysis has much in common with the investigation of stability of 2D surface states of disordered topological superconductors with respect to interactions [20,21]. A closely related

physics controls the enhancement of superconducting and ferromagnetic instabilities by disorder in 2D systems [23,52]. Further, there are close connections with the analysis of the anomalous scaling dimension of interactions in context of the study of decoherence and the dynamical critical exponent at the quantum-Hall transition with short-range interactions [53–55].

In the clean system, the relevance or irrelevance of an operator can be often established by a relatively straightforward power counting. As an example, this was done in Sec. IV to show that the interactions are RG-irrelevant at the clean fixed point of the Majorana chain. In the presence of disorder, the situation is much more complex, since the multifractal nature of wave functions as well as a nontrivial scaling of the density of states have to be taken into account. Formally, this disorder-induced renormalization of the interaction U can be expressed by an RG equation of the form [20,21]

$$\frac{d\ln U}{d\ln L} = x_1 - x_2^{(U)}. \tag{29}$$

Here, x_1 is the scaling dimension of the density of states of a noninteracting system, with $x_1 > 0$ and $x_1 < 0$ corresponding to the cases of vanishing and diverging density of states, respectively. Further, $x_2^{(U)}$ is the scaling dimension of the four-fermion interaction operator with respect to the noninteracting theory. For a detailed derivation of Eq. (29) we refer the reader to Appendix C of Ref. [21]. If the right-hand side of Eq. (29) is positive, the interaction is relevant at the noninteracting fixed point; otherwise it is irrelevant.

For a short-range interaction, and in the case when cancellations of the Hartree-Fock type (see below) are not operative, the scaling dimension $x_2^{(U)}$ is equal to the dimension x_2 of the squared density of states (which is also a local four-fermion operator). For the clean system, x_2 is simply equal to $2x_1$ but for a disordered system one has in general $x_2 < x_1$ in view of multifractality (characterizing strong fluctuations of the density of states) [21,56,57]. Specifically,

$$x_2 = \Delta_2 + 2x_1, \tag{30}$$

where $\Delta_2 < 0$ is the anomalous dimension of the fourth moment of the eigenfunction ($\langle U_{i\alpha}^4\rangle$ in the notations used below). In this situation of the maximally relevant interaction (no suppression due to Hartree-Fock cancellation or other reasons), Eq. (29) takes the form

$$\frac{d\ln U}{d\ln L} = -x_1 - \Delta_2. \tag{31}$$

The sum of two exponents $-x_1$ and $-\Delta_2$ in the right-hand side (r.h.s.) of Eq. (31) determines the scaling with L of the product νC_H of the density of states ν and the Hartree-type correlation function C_H [defined in Eq. (48) below] for $r = 0$.

In general, $x_2^{(U)} \geqslant x_2$ since the effect of the interaction can be suppressed due to Hartree-Fock-type cancellation. In this generic situation, we have, in analogy with Eq. (30),

$$x_2^{(U)} = \Delta_2^{(U)} + 2x_1, \tag{32}$$

where $\Delta_2^{(U)}$ is the anomalous dimension of the eigenstate correlation function $C_{\rm HF}$ corresponding to the matrix element of the interaction [and thus taking into account possible Hartree-Fock-type cancellations; see, e.g., Eq. (47) for the case of complex fermions below]. Substituting Eq. (32) into Eq. (29), we get

$$\frac{d\ln U}{d\ln L} = -x_1 - \Delta_2^{(U)}. \tag{33}$$

The sum of the exponents $-x_1$ and $-\Delta_2^{(U)}$ in the r.h.s. of Eq. (33) corresponds to the scaling with L of the product $\nu C_{\rm HF}$ of the density of states and the correlation function $C_{\rm HF}$. Below we determine the explicit form of this correlation function by inspecting the expectation value of the interaction operator and analyze the scaling of the product $\nu C_{\rm HF}$ with L for the models of complex fermions (Sec. V B) and for the Majorana model (Sec. V C).

If $-x_1 - \Delta_2^{(U)} < 0$, the interaction is RG-irrelevant, i.e., the noninteracting fixed point is stable with respect to inclusion of not too strong interaction. In the opposite case, $-x_1 - \Delta_2^{(U)} > 0$, the interaction is RG-relevant and drives the system away from the noninteracting fixed point. It was found in previous works on the effect of interaction at critical points of higher spatial dimensionality ($d > 1$, with a particular focus on 2D systems) [20–23,53–55] that both these scenarios can be realized. Whether the interaction is relevant or irrelevant depends on the specific noninteracting critical theory considered (i.e., spatial dimensionality as well as symmetry and topology class). As we show below, both scenarios are also realized in the context of the present work (1D critical systems of class BDI): the interaction is irrelevant in the case of complex fermions and relevant in the Majorana model.

The present problem has much in common with $d > 1$ Anderson-localization critical points studied in previous works where the multifractality induces strong correlations between eigenstates at different spatial points and different energies (often referred to as Chalker scaling). In fact, critical singularities are particularly strong in the present case. In the more conventional situation, both the density of states ν and the eigenstate correlation function $C_{\rm HF}$ (and, correspondingly, their product) exhibit a power-law scaling with L, so that the indices x_1 and $\Delta_2^{(U)}$ are constant (i.e., independent on L). On the other hand, we will see below that in the present problem ν and (in the complex-fermion case) $C_{\rm HF}$ scale exponentially with $\sqrt{L}$, which means that x_1 and $\Delta_2^{(U)}$ are L-dependent and increase (by absolute value) at large L as $\sqrt{L}/\ln L$. This is a manifestation of the fact that the 1D critical point studied here is characterized by very strong multifractality. What we are interested in is the sign of $-x_1 - \Delta_2^{(U)}$ at large L which controls the behavior (increase or decrease) of $\nu C_{\rm HF}$ in the limit $L \to \infty$.

For systems of the symmetry class BDI in one dimension with an odd number of channels, the density of states at low energies ϵ exhibits the well known Dyson singularity [36,58–60]:

$$\nu(\epsilon) \sim \frac{1}{\epsilon|\ln\epsilon|^3}. \tag{34}$$

We can use this result to calculate the position of the nth level in a system of the length L:

$$\int_0^{\epsilon_n} \nu(\epsilon)d\epsilon = \frac{n}{L}, \tag{35}$$

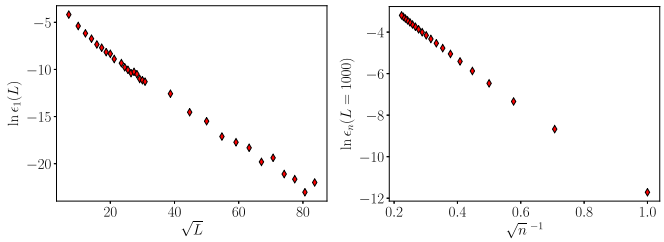

FIG. 14. Numerical verification of Eq. (36) for the scaling of energies of the low-lying single-particle states. (Left) Average energy of the lowest eigenstate ϵ_1 as a function of the square root of the system size, confirming the scaling $-\ln \epsilon_1 \propto \sqrt{L}$. (Right) Average energy ϵ_n of the nth eigenstate vs $1/\sqrt{n}$ in a system of size $L = 1000$, confirming the scaling $-\ln \epsilon_n \propto n^{-1/2}$ for sufficiently low energies. Combination of the scaling behavior observed in both panels confirms Eq. (36).

which yields

$$\epsilon_n \sim \exp\left(-c\sqrt{\frac{L}{n}}\right), \quad c = O(1). \tag{36}$$

We have verified the scaling (36) numerically for the model with the nearest-neighbor hopping matrix elements uniformly distributed over the interval $t_j \in [0, 1]$. The numerical data shown in Fig. 14 fully confirm the analytical prediction, with the coefficient $c \approx 0.5$. Thus we can write down the density of states around the lowest energy state ϵ_1 as a function of the length L:

$$\nu(0, L) \sim \frac{\exp(c\sqrt{L})}{L^{\frac{3}{2}}}. \tag{37}$$

This behavior is not of power-law type, i.e., it is not characterized by a critical exponent in the usual sense. We can define, however, an L-dependent scaling exponent $x_1(L) = -\partial \ln \nu / \partial \ln L$, with the result

$$-x_1(L) = c\frac{\sqrt{L}}{\ln(L)} - \frac{3}{2}. \tag{38}$$

The result (38) for the scaling dimension of the density of states is valid both for the Majorana and complex fermions, since these models are equivalent in the absence of interaction. (The only difference is that the number of states is halved in the case of Majoranas.) On the other hand, we will show that the scaling dimension $\Delta_2^{(U)}$ of the interaction is completely different in these two models. We will explore the scaling of interaction by a numerical approach, supporting the results by analytical arguments.

A. Scaling of interactions

In order to determine the scaling of the interaction operators, we express the interaction matrix elements in terms of linear combinations of products of single-particle eigenfunctions. These expression in terms of the eigenfunctions are then numerically averaged over the disorder. The numerical results will be also supported by analytical considerations (Appendix D).

We start by writing the most general noninteracting Hamiltonian of a 1D system of size L of symmetry class BDI [56]:

$$H = \frac{1}{2}(\mathbf{c}_A^\dagger \quad \mathbf{c}_B^\dagger)\begin{pmatrix} 0 & \underline{h} \\ \underline{h} & 0 \end{pmatrix}\begin{pmatrix} \mathbf{c}_A \\ \mathbf{c}_B \end{pmatrix}, \tag{39}$$

where $\underline{h}$ is a real matrix and $c_{A,B}$, $c_{A,B}^\dagger$ are onsite operators acting on the two sublattices. In the case of the complex fermionic chain, these are fermionic creation and annihilation operators, in the case of the Majorana chain we have $c_A = \gamma_A = c_A^\dagger$ and $c_B = i\gamma_B = -c_B^\dagger$, where $\gamma_{A,B}$ are the real Majorana operators in Eq. (12). Diagonalizing the $L \times L$ matrix in Eq. (39), one can rewrite the Hamiltonian in the basis of operators which correspond to the single particle excitations of the system,

$$H = \frac{1}{2}(\mathbf{d}_+^\dagger \quad \mathbf{d}_-^\dagger)\begin{pmatrix} \underline{\epsilon} & 0 \\ 0 & -\underline{\epsilon} \end{pmatrix}\begin{pmatrix} \mathbf{d}_+ \\ \mathbf{d}_- \end{pmatrix}, \tag{40}$$

$$c_i = \sum_\alpha U_{i,\alpha} d_\alpha. \tag{41}$$

Here, $\underline{\epsilon}$ is a diagonal matrix with eigenvalues $0 < \epsilon_1 < \epsilon_2 < \ldots < \epsilon_{L/2}$. In the case of complex fermions, the eigenvectors $U_{i\alpha}$ are just the conventional single-particle wave function $\Psi_\alpha(i)$. The ground state $|\Omega\rangle$ of the Hamiltonian can be written in terms of the operators d and the zero-particle state $|0\rangle$:

$$|\Omega\rangle = \prod_{\alpha, \epsilon_\alpha < 0} d_\alpha^\dagger |0\rangle. \tag{42}$$

This immediately yields the action of the d operators on the ground state:

$$d_\alpha |\Omega\rangle = 0, \quad \text{for} \quad \epsilon_\alpha > 0, \tag{43}$$

$$d_\alpha^\dagger |\Omega\rangle = 0, \quad \text{for} \quad \epsilon_\alpha < 0. \tag{44}$$

A general q-body interaction operator can be expressed as sum of products of annihilation and creation operators of the following type:

$$\hat{O} = \prod_{i=1}^{q} c_{a_i}^\dagger \prod_{j=q+1}^{2q} c_{a_j}$$

$$= \sum_{\{\alpha_i, \alpha_j\}} \prod_{i=1}^{q} U_{a_i,\alpha_i} d_{\alpha_i}^\dagger \prod_{j=q+1}^{2q} U_{a_j,\alpha_j} d_{\alpha_j}. \tag{45}$$

The expectation value of the operator $\hat{O}$ over any eigenstate of a noninteracting system can now be calculated by substituting Eq. (41) into Eq. (45):

$$\langle \hat{O} \rangle = \sum_{\{\alpha_i, \alpha_j\}} \prod_{i,j} U_{a_i,\alpha_i} U_{a_j,\alpha_j} \left\langle \prod_{i=1}^{q} d_{\alpha_i}^\dagger \prod_{j=q+1}^{2q} d_{\alpha_j} \right\rangle. \tag{46}$$

The expectation value that stands as a last factor on the right-hand side of Eq. (46) is nonzero only if the states α_i and α_j are pairwise identical; in this case, it is equal to $+1$ or -1, depending on parity of the permutation of indices. The right-hand side of Eq. (46) thus represents an algebraic sum of products of single-particle eigenfunctions.

The terms in Eq. (46) are therefore the matrix elements of the interaction operator expressed as products of the eigenvector amplitudes $U_{i\alpha}$. For the conventional case of two-body interaction, $q = 2$, on which we focus below, Eq. (46) reduces, in accordance with the Wick theorem,to a sum over pairs of states α_1, α_2. For a given choice of sites $a_1, \ldots, a_4$ and eigenstates α_1 and α_2, there will be two different terms in Eq. (46) (plus analogous terms obtained by an interchange $\alpha_1 \leftrightarrow \alpha_2$), that have a meaning of Hartree and Fock terms. These two terms correspond to the order of subscripts $\alpha_1\alpha_2\alpha_1\alpha_2$ and $\alpha_1\alpha_2\alpha_2\alpha_1$ of d operators in Eq. (46). As usual, the Fock term will enter with a relative minus sign due to Fermi statistics. We will see below that, in close analogy with Refs. [53–55], a major cancellation between the Hartree and Fock terms will play a crucial role for the RG irrelevance of the interaction in the case of complex fermions. In the case of Majorana system, there is a third term, originating from the following order of indices $\alpha_1\alpha_1\alpha_2\alpha_2$, as discussed in detail in Sec. V C. It has a meaning of the Cooper term, and its emergence it is not surprising since Majorana excitations are characteristic for superconducting systems. As we show below, the presence of this term spoils the cancellation, making the total interaction matrix element relevant in the RG sense.

In general, the disorder averaged value of matrix elements under consideration is a function of the system size and of the energies of the $q = 2$ eigenvectors involved. To obtain the scaling of these functions numerically, matrices of the form Eq. (39) for different system sizes were generated and the lowest 20 eigenvectors calculated. Then for each pair of eigenvectors the corresponding matrix elements entering Eq. (46) were calculated. This procedure yields pairs of energies and the associated matrix elements, which then have to be averaged over disorder configurations. This is done by making a histogram and averaging the matrix elements over each energy bin. It is worth emphasizing that for the cases of logarithmic dependence of the matrix elements on energy, the correct choice of averaging procedure is crucial. In these cases, the bin sizes are chosen such that the number of data points is the same in every bin.

Even though we deal here with eigenstates of a noninteracting problem, the corresponding numerical analysis is a rather challenging endeavour. This is particularly true in the regime of strong Hartree-Fock cancellations that plays a central role below. In this situation, the default double precision that provides approximately 15 decimal digits is by far insufficient. As will be shown below, the Hartree and Fock terms can be the same within hundreds of digits for large systems. The calculations have therefore been performed with at least 500 decimal digit floating point arithmetics.

Since for large ($L \gg 1$) systems full diagonalization becomes slow [typically $\mathcal{O}(L^3)$] and memory intensive [at least $\mathcal{O}(L^2)$], a transfer matrix approach is chosen to compute the first few eigenvectors U_{i,ϵ_i}. The characteristic polynomial $\lambda(\epsilon)$ is evaluated by L column expansions in $\mathcal{O}(L^2)$. The first 20 eigenenergies ϵ_i closest to zero are obtained as roots of $\lambda(\epsilon)$. The ϵ_i are plugged into the transfer matrix equation (B1) to find U_{i,ϵ_i}. For all following calculations, the hopping parameters are chosen to be uniformly distributed over the interval $t_j \in [0, 1]$.

B. Complex fermion chain

We start with the model of the complex fermionic chain described by Hamiltonian (2). Due to chiral symmetry, each state with positive energy has a partner state with negative energy. For zero chemical potential, in the noninteracting ground state, all states of negative energy are occupied and all of positive energy are free. The relevance of the interaction in the infrared limit is controlled by its matrix elements evaluated on low-lying eigenstates. To obtain the appropriate eigenstate correlation function, we inspect the expectation value of the interaction, Eq. (46). For each pair of sites i and j, we have a contribution

$$\begin{aligned}\langle c_i^\dagger c_{i+r}^\dagger c_i c_{i+r}\rangle &= \sum_{\alpha\beta\gamma\delta} U_{i\alpha}U_{i\beta}U_{i+r,\gamma}U_{i+r,\delta}\langle d_\alpha^\dagger d_\beta^\dagger d_\gamma d_\delta\rangle \\ &= \sum_{\{\alpha\beta\}}(U_{i\alpha}U_{i\alpha}U_{i+r,\beta}U_{i+r,\beta} \\ &\quad - U_{i\alpha}U_{i\beta}U_{i+r,\alpha}U_{i+r,\beta}),\end{aligned} \tag{47}$$

with the summation in the last expression going over pairs of filled states. The two terms in brackets after the last equality sign in Eq. (47) correspond to the conventional Hartree and Fock diagrams. We define the corresponding correlation functions of two single-particle eigenfunctions as functions of energies, distance, and system size:

$$C_{\mathrm{H}}(\epsilon_\alpha, \epsilon_\beta, r, L) = \langle U_{i\alpha}U_{i\alpha}U_{i+r,\beta}U_{i+r,\beta}\rangle_{\mathrm{dis}}, \tag{48}$$

$$C_{\mathrm{F}}(\epsilon_\alpha, \epsilon_\beta, r, L) = \langle U_{i\alpha}U_{i\beta}U_{i+r,\alpha}U_{i+r,\beta}\rangle_{\mathrm{dis}}, \tag{49}$$

$$\begin{aligned}C_{\mathrm{HF}}(\epsilon_\alpha, \epsilon_\beta, r, L) = \langle &U_{i\alpha}U_{i\alpha}U_{i+r,\beta}U_{i+r,\beta} \\ &- U_{i\alpha}U_{i\beta}U_{i+r,\alpha}U_{i+r,\beta}\rangle_{\mathrm{dis}},\end{aligned} \tag{50}$$

where $\langle\ldots\rangle_{\mathrm{dis}}$ denotes the disorder averaging. Below, we analyze the scaling of the full correlation function $C_{\mathrm{HF}} = C_{\mathrm{H}} - C_{\mathrm{F}}$ in order to determine the scaling exponent $\Delta_2^{(U)}$ of the interaction. It was verified in Refs. [53–55] that this scaling dimension also controls the scaling of interaction matrix elements also in the second order of the perturbation theory. We thus expect that that the analysis of the scaling of the correlation function (50) with energy and the distance is sufficient for establishing the relevance or irrelevance of the interaction near the noninteracting fixed point.

The following comment concerning the r dependence is in order here. Our DMRG results above dealt with short range interaction $r \sim 1$ only. At the same time, one may be also interested in effects of long-range interaction, in which case one needs to know the scaling of correlations functions of the type (50) with r. Furthermore, the analysis of correlations of eigenstates at the infinite-randomness fixed point constitutes by itself a very interesting problem (with r dependence being an important ingredient), as it represents a remarkable example of strong-coupling Anderson-localization critical point (see also a discussion in Sec. VI). Since the r dependence of the correlation functions (48)–(50) can be tackled by the same approach, we analyze below the correlation functions not only for $r \sim 1$ but also for arbitrary r. In the end, when we study the RG relevance of the short-range interaction, we focus on the correlations at $r \sim 1$. This comment applies also to the Majorana chain, Sec. V C.

1. Single-wave-function correlations

Terms where the two wave functions are identical, i.e., $\alpha = \beta$, do not contribute to the interaction matrix element C_{HF} as the Hartree and Fock terms cancel each other exactly. Nevertheless, it is useful to start our analysis by considering the single-wave-function correlations for two reasons. First, they can be particularly well understood analytically and can serve as a benchmark to our numerical calculations. Second, we will see below that some of properties of the single-wave-function correlations translate to correlations of two eigenstates that are important for the interacting models. We define the two-point, single-wave-function correlation function C_2:

$$C_2(\epsilon_\alpha, r, L) = \langle U_{i\alpha} U_{i\alpha} U_{i+r,\alpha} U_{i+r,\alpha} \rangle_{\mathrm{dis}}. \tag{51}$$

For zero energy, the wave function U_r can be expressed exactly in terms of a given realization of disorder [36]. The zero-energy wave functions belong entirely to one of the two sublattices (i.e., vanish on the other sublattice). If one looks at the wave-function moments at a single point, their scaling is similar to that of a fully localized wave function [36,56]:

$$\left\langle U_r^{2q} \right\rangle \sim \frac{1}{L}, \tag{52}$$

for $q > 0$. At the same time, the spatial decay of the correlation function C_2 at zero energy is only algebraic, which is a property of a critical system [36]:

$$C_2(0, r, L) \sim \begin{cases} r^{-\frac{3}{2}} L^{-1}, & r \text{ even}; \\ 0 & r \text{ odd}. \end{cases} \tag{53}$$

For finite energy, this formula for even-r correlations is expected to hold as long as the distance r is smaller than the localization length, $r \lesssim \xi_\epsilon$. The latter was predicted [36] to scale with energy as

$$\xi_\epsilon \propto |\ln \epsilon|^2. \tag{54}$$

Using Eq. (36) with $n = 1$, we see that $\xi_\epsilon \sim L$ for the lowest eigenstate.

As to odd-distance correlations, they are not exactly zero for a nonzero energy ϵ. Indeed, the absence of odd-distance correlations, Eq. (53), is a consequence of the chiral symmetry which is exact at $\epsilon = 0$ but is violated at nonzero energy and gets progressively more strongly broken when the energy increases. Thus the odd-r correlations should be strongly suppressed relative to even-r correlations at low energies, with the suppression becoming stronger with lowering energy. As shown in Appendix B, the corresponding suppression factor is $\sim \epsilon^2$ for odd $r \sim 1$.

We confront now the analytical predictions with numerical simulations. In Fig. 15, we plot there the r dependence of the correlation function $C_2(\epsilon_1, r, L = 400)$, separately for even and odd r. For even r, we observe the $r^{-3/2}$ scaling, in agreement with Eq. (53). This scaling holds with a good accuracy up to $r \approx L/2$. As to the odd-distance correlations, they are strongly suppressed for small r in comparison to even-distance ones, again in consistency with theoretical expectations. Curiously, when r approaches the system size L, the odd correlations become much stronger that the even correlations. This behavior will, however, play no role for our analysis, since we consider a finite-range interaction, i.e., $r \sim 1$.

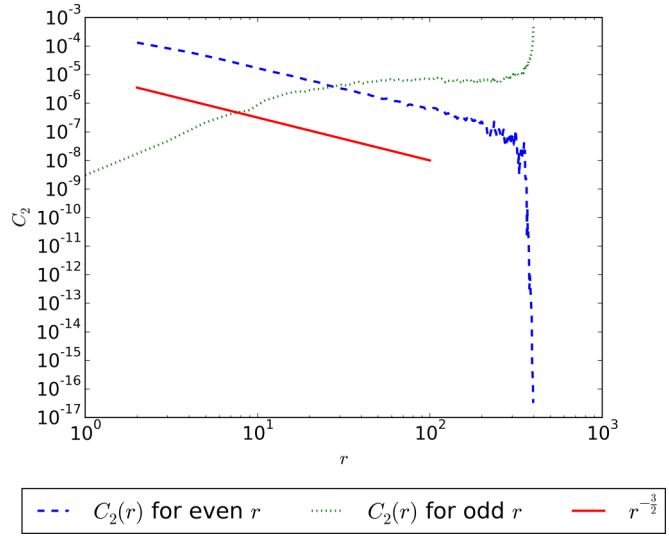

FIG. 15. Single-wave-function correlation function $C_2(\epsilon_1, r, L = 400)$ vs distance r for the lowest-energy state in a disordered complex-fermion chain of size $L = 400$, for even and odd distances r. For small even distances, C_2 scales as $r^{-3/2}$ in agreement with Eq. (53). At distances r approaching L even correlations are strongly suppressed. Odd correlations are strongly suppressed for small distances in consistency with Eq. (53) and with the result of Appendix B but become large for r comparable to L.

In Fig. 16, we show the numerically obtained energy dependence of the correlation function C_2 for fixed $L = 1200$ and fixed small separation r. Specifically, we choose $r = 2$ for the even case and $r = 1$ for the odd case. It is seen that the even-distance correlations are essentially independent of ϵ. This is the expected behavior: indeed, for $r \sim 1$, the condition $r \ll \xi_\epsilon$ is fulfilled as long as $|\ln \epsilon| \gg 1$, i.e., essentially in the whole range of $\ln \epsilon$. On the other hand, the odd-distance correlations strongly increase with energy. Specifically, the data

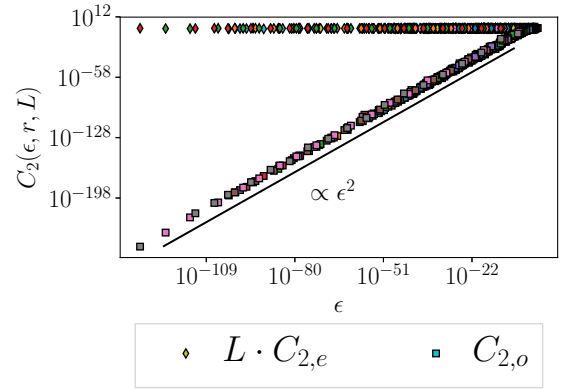

FIG. 16. Single-wave-function correlation function for short even distance, $LC_2(\epsilon, r = 2, L)$, and short odd distance, $C_2(\epsilon, r = 1, L)$, vs energy ϵ in systems with size L from 100 to 10 000 (distinct colors). For $r = 2$, the correlation function is independent on energy, while for $r = 1$, it scales as ϵ^2 (and thus is strongly suppressed at low energy), as predicted analytically.

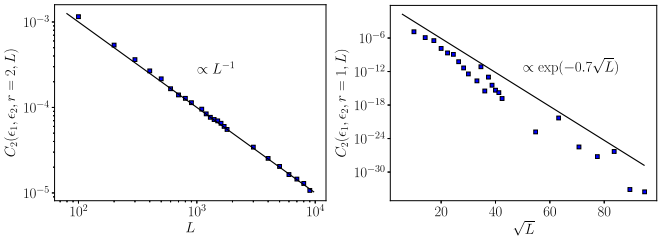

FIG. 17. Single-wave-function correlation function for short even distances $C_2(\epsilon_1, r = 2, L)$ (left) and short odd distances $C_2(\epsilon_1, r = 1, L)$ (right) vs system size L. For $r = 2$, the data confirm the analytically predicted scaling, $C_2 \sim L^{-1}$, see first line of Eq. (53). For odd distance, the correlation function decreases quickly with L since the lowest energy ϵ_1 approaches zero exponentially fast, $\epsilon_1 \sim \exp(-c\sqrt{L})$ and in view of $C_2 \propto \epsilon_1^2$, see Appendix B.

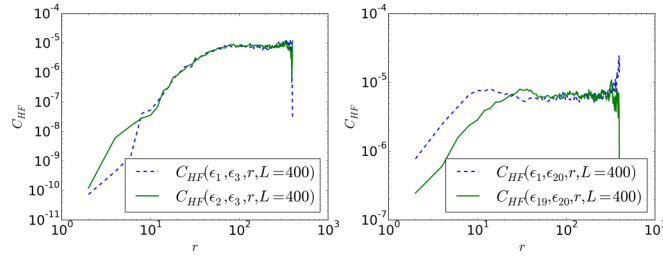

FIG. 18. (Left) $C_{\rm HF}(\epsilon_1, \epsilon_3, r, L = 400)$ and $C_{\rm HF}(\epsilon_2, \epsilon_3, r, L = 400)$ as functions of the even distance r. Two curves are essentially identical, which confirms insensitivity of the correlation function to the lower energy, as long it is much smaller than the larger one. (Right) $C_{\rm HF}(\epsilon_1, \epsilon_{20}, r, L = 400)$ and $C_{\rm HF}(\epsilon_{19}, \epsilon_{20}, r, L = 400)$ as functions of the even distance r. The two curves show again a similar behavior but now there is a difference in a factor of order unity ($\approx$3) between them at small r. This is because in this plot we consider higher-energy state, and, in particular, ϵ_{19} is close to ϵ_{20}.

unambiguously demonstrate the ϵ^2 behavior of $C_2(\epsilon, r, L)$ for small odd r discussed above and derived analytically in Appendix B. It is worth emphasizing the enormously broad range of variation of the energy ϵ and the correlation function C_2 (odd r) in Fig. 16: about 130 and 260 orders of magnitude, respectively!

Finally, in Fig. 17, we show dependence of the correlation function $C_2(\epsilon_1, r, L)$ on the system size L for even ($r = 2$) and odd ($r = 1$) distance. In the even case, the correlation function does not depend on energy for small r, so that the fact that ϵ_1 is different from zero and varies with L is of no importance. The expected result is given by the first line of Eq. (53). The numerical data in the right panel of Fig. 17 confirm the predicted L^{-1} scaling. For odd r the decay of $C_2(\epsilon_1, r, L)$ with L should be exponentially fast due to $C_2(\epsilon, r, L) \sim \epsilon^2$ and the fact that the energy ϵ_1 approaches zero exponentially with increasing L, see Eq. (36). This yields the analytical expectation $C_2(\epsilon_1, r, L) \sim \exp(-2c\sqrt{L})$, in full agreement with the data in the right panel of Fig. 17.

2. *Two-wave-function correlations*

Matrix elements for two-wave-function correlations, Eqs. (48)–(50), are calculated using two eigenstates with different energies for a given disorder configuration, and then averaging over disorder. The energy levels are on average distributed as $\epsilon_n \sim \exp(-c\sqrt{L/n})$, which means that, for $L \gg 1$ and $n \sim 1$, one of the energies will almost always be much larger than the other one. Since the energy breaks the chiral symmetry, it is expected that the matrix elements will essentially depend only on the larger of the two energies and only weakly on the lower one. To verify numerically this expectation, we compare in the left panel of Fig. 18 the Hartree-Fock correlation functions [see Eq. (50)] $C_{\rm HF}(\epsilon_1, \epsilon_3, r, L = 400)$ of the lowest and third lowest energy levels with $C_{\rm HF}(\epsilon_2, \epsilon_3, r, L = 400)$ of the second lowest and the third lowest energy levels, for even r. As we will show below, this correlation function exhibits, for low energies, very strong dependence on the higher of the two energies. At the same time, the two curves in the left panel of Fig. 18 are nearly identical (within statistical fluctuations), which confirms the essential insensitivity to the value of the lower energy. In the right panel of Fig. 18, we show analogous data by choosing now a higher excited state ϵ_{20} and varying the state with lower energy from ϵ_1 to ϵ_{19}. One still expects to see the same scaling behavior for the two correlation functions; however, since ϵ_{19} and ϵ_{20} are nearly equal for this value of L, a difference in a numerical factor of order unity is expected. This is exactly what is observed in the right panel of Fig. 18. In the numerical analysis below, we will choose the state with the lowest energy (ϵ_1) as one of the two states for which the correlation function is calculated. This energy is always much smaller than another eigenstate energy (that will be denoted as ϵ), which simplifies the scaling analysis at criticality.

The correlation functions at criticality depend thus on the energy ϵ, the length L, and the distance r. As for the single-eigenstate correlation function, Sec. V B 1, the behavior for even and odd distances r is very different. At low energy ϵ, and short even distances, it is natural to expect that C_H behaves, in similarity with with C_2, as a power law in r and L. Such a power-law behavior is also analogous to that of eigenfunction correlation functions at critical points of localization-delocalization transitions in systems of higher dimensionality, see Ref. [56]. As to the expected for of the energy dependence, we recall that, at the critical point that we study, the logarithm of the energy scales as a power law of the length, see Eq. (36). Therefore it is natural to expect a power-law scaling of C_H with respect to $\ln \epsilon$. Therefore, for short even distances r and low energy ϵ, the correlation function C_H is expected to have the scaling form (see also Ref. [61]):

$$C_H(0, \epsilon, r, L) \sim \frac{|\ln \epsilon|^\alpha}{r^\beta L^\gamma}, \quad r \text{ even}. \tag{55}$$

This equation should hold at criticality, so that the necessary condition is $r \lesssim \xi_\epsilon$. We determine now the exponents α, β, and γ by a numerical analysis. We will also support the numerical results by analytical considerations (details of which are presented in Appendix D) yielding the values of the exponents α and γ.

In the left panel of Fig. 19, the numerically obtained dependence of the correlation functions on r is shown for even r. We see that C_H at not too large r scales $r^{-\beta}$ with $\beta = 3/2$. This scaling is the same as for the single-eigenfunction correlation

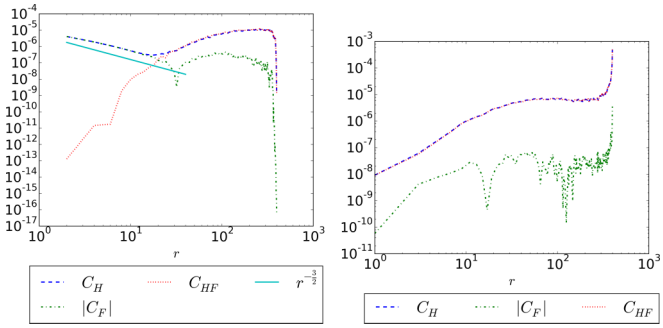

FIG. 19. Hartree, $C_H(\epsilon_1, \epsilon_2, r, L = 400)$, and Fock, $C_F(\epsilon_1, \epsilon_2, r, L = 400)$, correlation functions and their difference $C_{\rm HF}(\epsilon_1, \epsilon_2, r, L = 400)$ plotted as functions of the distance r. (Left) Even r. The scaling of C_H at criticality (distance r much smaller than the correlation length ξ_ϵ), is of the $r^{-\frac{3}{2}}$ form, implying that the index β in Eq. (55) is $\beta = 3/2$. The Fock term is nearly equal to the Hartree term in this critical regime, so that $C_{\rm HF}$ is very strongly suppressed at small r. At $r \approx 40$, the Fock term becomes much smaller than the Hartree one and changes sign. (Right) Odd r. In the critical regime (small r) the Hartree term is strongly suppressed. The Fock term is still smaller, so that $C_{\rm HF} \simeq C_H$.

function C_2, see Sec. V B 1. To find the exponent α in the critical scaling of C_H, Eq. (55), we show in the right panel of Fig. 20 the dependence of correlation functions at small even distance ($r = 2$) and fixed L on the energy. The slope yields $\alpha = 1$. To determine γ, we plot in the left panel of the same figure the dependence on the system size L. Here the

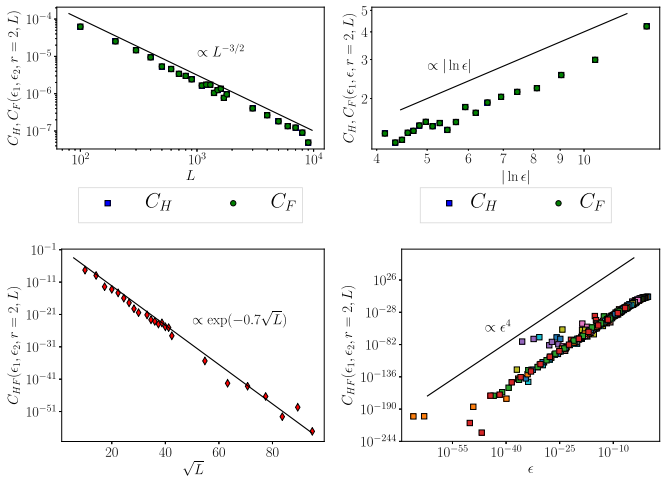

FIG. 20. Hartree, Fock, and Hartree-Fock correlation functions $C_H(\epsilon_1, \epsilon, r = 2, L)$, $C_F(\epsilon_1, \epsilon, r = 2, L)$, and $C_{\rm HF}(\epsilon_1, \epsilon, r = 2, L)$ for a small even distance ($r = 2$). (Upper left) Scaling of C_H, C_F with L at $\epsilon = \epsilon_2$. The slope yields the power-law scaling $\sim L^{-3/2}$, implying a relation $\gamma - \alpha/2 = 3/2$ for the exponents in Eq. (55). (Upper right) Scaling with energy at fixed $L = 4000$. The slope implies the scaling $\sim|\ln\epsilon|$ for C_H, implying the exponent $\alpha = 1$ in Eq. (55). In both panels, the Fock correlation function is nearly equal to the Hartree one, which is a characteristic feature of the critical regime for even r. As a result, $C_{\rm HF}$ shown in lower panels is strongly suppressed with respect to C_H and C_F. (Lower left) Scaling of $C_{\rm HF}$ with L at $\epsilon = \epsilon_2$. (Lower right) Scaling of $C_{\rm HF}$ with energy for L from 100 to 10 000. The slope agrees with the analytical prediction $C_{\rm HF} \propto \epsilon^4$.

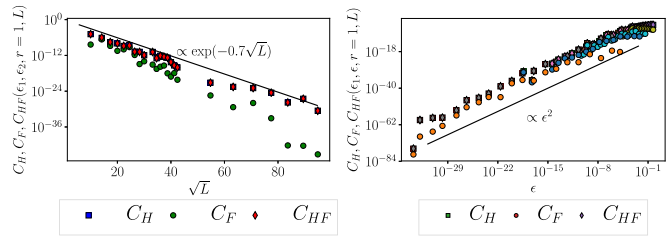

FIG. 21. Hartree, Fock, and Hartree-Fock correlation functions $C_H(\epsilon_1, \epsilon, r = 1, L)$, $C_F(\epsilon_1, \epsilon, r = 1, L)$, and $C_{\rm HF}(\epsilon_1, \epsilon, r = 1, L)$ for a small odd distance ($r = 1$). (Left) Scaling with L at $\epsilon = \epsilon_2$. (Right) Scaling with energy. Different colors represent different lengths from 100 to 10 000. In both panels, the Fock correlation function is much smaller than the Hartree one, so that $C_{\rm HF} \simeq C_H$. The dominant scaling for both C_H and C_F is $\sim\epsilon^2$ (which translates into an exponential length dependence in the left panel). The data for the Fock term suggest an additional power-law dependence on length.

correlation functions are evaluated for two lowest eigenstates, so that the energy ϵ is equal to $\epsilon_2 = \exp(-c\sqrt{L/2})$. The obtained scaling of C_H is L^{-2}; taking into account the $|\ln\epsilon_2| \sim L^{1/2}$ factor originating from the energy dependence of C_H, we find that $\gamma = 2$. The scaling of C_H in the critical regime is thus given by

$$C_H(0, \epsilon, r, L) \sim \frac{|\ln\epsilon|}{L^2 r^{\frac{3}{2}}}, \quad r \text{ even}. \tag{56}$$

The Fock correlation function C_F for even r is found to behave in exactly the same way. This is what should be expected: indeed, a particular case of a small even r is $r = 0$, for which C_H and C_F are identically the same. The $|\ln\epsilon|L^{-2}$ scaling of C_H and C_F for even r is confirmed also by an analytical calculation of the averaged square of the Green function, see Appendix D for details.

As was discussed above, the effect of the interaction is controlled by the scaling of the Hartree-Fock correlation function $C_{\rm HF} = C_H - C_F$. As the data in Fig. 20 clearly demonstrate, this function is strongly suppressed (for small even r) as compared to C_H and C_F. This is also what is expected analytically: as shown in Appendix B, the suppression factor is $\sim\epsilon^4$. If the correlation function is evaluated for two lowest eigenstates, the suppression factor becomes $\sim\epsilon_2^4 \sim \exp(-4c\sqrt{L/2})$. These analytical predictions are fully confirmed by the numerical results, see Fig. 20.

We turn now to the critical behavior of the correlation functions at odd r. We expect that odd-distance correlation functions C_H and C_F are suppressed with respect to their even-r counterparts. The reason for this is the same as for the single-eigenfunction correlation function C_2, Sec. V B 1: odd-r correlations necessarily involve wave functions on different sublattices. As shown in Appendix B, the suppression factor for C_H and C_F with odd r is the same ($\sim\epsilon^2$) as for C_2. Again, this translates into an exponential suppression with respect to L.

This expectation is fully supported by the numerical results shown in Fig. 21. Note that, in the case of odd r, the Fock term is considerably smaller than the Hartree one (even though the dominant scaling factor is the same). This, the Hartree-Fock cancellation is not operative and $C_{\rm HF} \simeq C_H$.

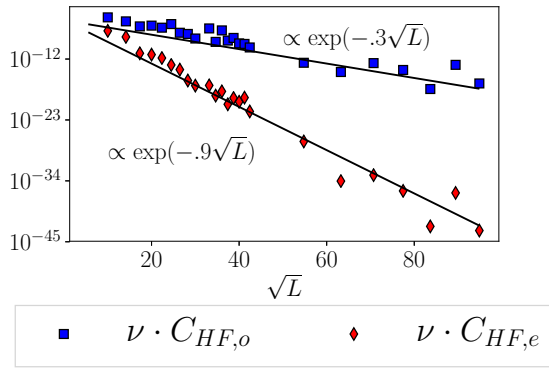

FIG. 22. RG irrelevance of interaction at the infinite-randomness fixed point of the complex-fermion chain. Product $\nu(L)C_{\rm HF}(\epsilon_1, \epsilon_2, r, L)$ of the Hartree-Fock matrix element at criticality multiplied by the density of states plotted vs the system size L, for odd ($r = 1$, blue symbols) and even ($r = 2$, red symbols). Both for even and odd distances, the product decreases quickly with L (as an exponential of $\sqrt{L}$), implying that the interaction is irrelevant.

We have thus found that the Hartree-Fock correlation function $C_{\rm HF}$ is strongly suppressed at criticality (i.e., at short distances r and low energies, so that $r \ll \xi_\epsilon$). This is valid both for even distances (due to cancellation between the Hartree and Fock terms) and for odd distances (due to different sublattices entering). The suppression factor is $\sim\epsilon^4$ for even r and $\sim\epsilon^2$ for odd r.

We can return now to the question of RG relevance of the interaction which is determined by Eq. (29). The right-hand side of this equation characterizes the scaling of the product of the interaction matrix element and the density of states with the system size L. The matrix element to be used here is the Hartree-Fock correlation function, see Eqs. (47) and (50). If this product increases (decreases) with L, the interaction is relevant (respectively, irrelevant). The density of states increases exponentially with $\sqrt{L}$ according to Eq. (37) or, equivalently, as $1/\epsilon$ with energy (up to logarithmic correction), see Eq. (34). On the other hand, the Hartree-Fock correlation function decreases as ϵ^2 (odd r) or ϵ^4 (even r). Thus the suppression of the Hartree-Fock correlation function is stronger than the increase of the density of states, and the product decays as a power of ϵ (and thus exponentially with respect to $\sqrt{L}$). To illustrate this, we plot in Fig. 22 the product $\nu(L)C_{\rm HF}(\epsilon_1, \epsilon_2, r, L)$ for small even and odd distances ($r = 2$ and 1, respectively) as a function of L. We see that both functions decrease exponentially with $\sqrt{L}$ as expected. This implies that the interaction in Eq. (2) is irrelevant in the presence of disorder, and the system stays critical (at the infinite-randomness fixed point), at least for sufficiently weak interaction. This is in agreement with our DMRG results in Sec. III and with real-space RG findings of Refs. [35,37].

We have focused above on the behavior of two-eigenstate correlation functions at criticality ($r \ll \xi_\epsilon$), since such functions emerge when one explores the effect of short-range interaction ($r \sim 1$). On the other hand, the behavior of the correlation functions at $r \gtrsim \xi_\epsilon$ may be of interest in other contexts. We briefly discuss this behavior in Appendix F.

C. Majorana chain

We turn now to the Majorana model. The simplest interaction term in this model was presented in Eq. (13). However, as was already mentioned before, any fourth order interaction term containing an even number of Majoranas on even sites (and an even number of those on on odd sites) is consistent with the symmetries of the Hamiltonian. In fact, such terms will be generated by RG even if one starts from the simplest term only as in Eq. (13).

We generalize first the interaction in Eq. (13) by introducing a distance r separating two nearest-neighbor pairs of Majoranas:

$$H_{\rm int} = \sum_{j=1}^{L} \gamma_j \gamma_{j+1} \gamma_{j+r} \gamma_{j+r+1}. \tag{57}$$

(We will assume $r \geqslant 2$ to be even but it is not particularly important here). Such a term is analogous to the odd-r interaction term in the case of complex fermions, see Eq. (3), since it involves two operators on even sites and two on odd sites.

We express the Majorana operators γ_i in terms of the Bogoliubov operators d_α using the definitions $c_A = \gamma_A = c_A^\dagger$ and $c_B = i\gamma_B = -c_B^\dagger$, and then diagonalizing the Hamiltonian matrix, see Sec. V A. At variance with the complex fermion case, these $2L$ Bogolyubov operators are not independent: each operator is related to its chiral conjugate with inverse sign of the energy, $d_\alpha^\dagger = d_{\bar\alpha}$. Thus we can express the Majorana operators by using only wave functions and Bogolyubov operators associated with positive energies:

$$\gamma_j = \sum_{\epsilon_\alpha > 0} U_{\alpha,j}(d_\alpha + d_\alpha^\dagger) \qquad (j \text{ even}), \tag{58}$$

$$\gamma_j = \sum_{\epsilon_\alpha > 0} iU_{\alpha,j}(d_\alpha - d_\alpha^\dagger) \qquad (j \text{ odd}). \tag{59}$$

Via the same token, the whole Hilbert space of the problem is obtained by acting with operators $d_\alpha^\dagger$ with $\epsilon_\alpha > 0$ on the vacuum state.

Substituting Eq. (59) into an interaction term in (57), one can evaluate the expectation value of the interaction term over any basis state of the noninteracting Fock space. For example, averaging over the noninteracting vacuum (that is annihilated by all d_α with positive energies), we get

$$\begin{aligned}\langle \gamma_k \gamma_{k+1} \gamma_{k+r} \gamma_{k+r+1} \rangle &= -\sum_{\alpha>0;\beta>0} (U_{k,\alpha} U_{k+1,\alpha} U_{k+r,\beta} U_{k+r+1,\beta} \\ &\quad + U_{k,\alpha} U_{k+1,\beta} U_{k+r,\alpha} U_{k+r+1,\beta} \\ &\quad - U_{k\alpha} U_{k+1\beta} U_{k+r,\beta} U_{k+r+1,\alpha}).\end{aligned} \tag{60}$$

Three terms here correspond to the expansion of a Pfaffian that is a general form of the Majorana Wick's theorem [62].

The matrix element in Eq. (60) consists of three terms. The first of them is similar to a Hartree term in the sense that amplitudes of each eigenstates enter at spatial points separated by a minimal distance (one site). The other two terms are similar to Fock terms. In full analogy with the case of complex fermions, we define correlation functions depending on two

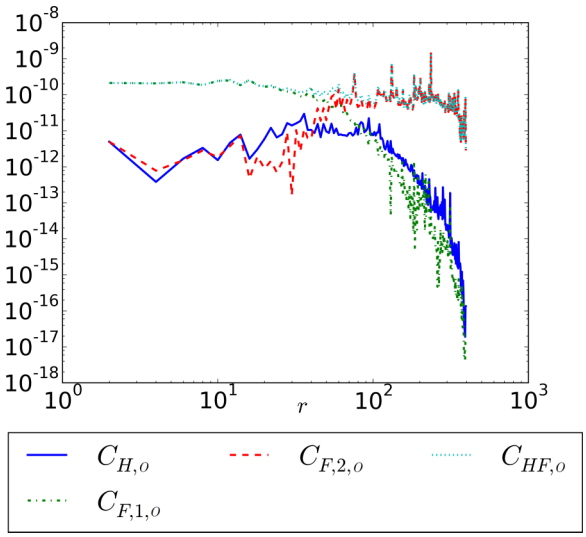

FIG. 23. Eigenstate correlation functions (61)–(64) corresponding to the four-point Majorana interaction for two lowest-energy eigenstates with even $r \geqslant 2$ in the system of size $L = 400$. For sufficiently short distances, $r < \xi_\epsilon$ (critical regime), the term $C_{F,1,o}$ is dominant and r-independent. The magnitude of all terms is rather small in view of the ϵ^2 suppression that is demonstrated in Fig. 24.

energies, distance r, and the system size L: ϵ_α, ϵ_β, system size L and distance r:

$$C_{H,o}(\epsilon_\alpha, \epsilon_\beta, r, L) = \langle U_{k,\alpha} U_{k+1,\alpha} U_{k+r,\beta} U_{k+r+1,\beta} \rangle_{\rm dis}, \tag{61}$$

$$C_{F,1,o}(\epsilon_\alpha, \epsilon_\beta, r, L) = \langle U_{k,\alpha} U_{k+1,\beta} U_{k+r,\alpha} U_{k+r+1,\beta} \rangle_{\rm dis}, \tag{62}$$

$$C_{F,2,o}(\epsilon_\alpha, \epsilon_\beta, r, L) = \langle U_{k,\alpha} U_{k+1,\beta} U_{k+r,\beta} U_{k+r+1,\alpha} \rangle_{\rm dis}, \tag{63}$$

$$\begin{aligned} C_{HF,o}(\epsilon_\alpha, \epsilon_\beta, r, L) = &\langle U_{k,\alpha} U_{k+1,\alpha} U_{k+r,\beta} U_{k+r+1,\beta} \\ &+ U_{k,\alpha} U_{k+1,\beta} U_{k+r,\alpha} U_{k+r+1,\beta} \\ &- U_{k,\alpha} U_{k+1,\beta} U_{k+r,\beta} U_{k+r+1,\alpha} \rangle_{\rm dis}. \end{aligned} \tag{64}$$

The subscript "o" serves to indicate that, as was explained above, these correlation functions bear analogy with odd-r correlations introduced for the model of complex fermions.

The same analytical consideration as were used in the case of correlation functions (48)–(50) with odd r suggest that all the correlation functions (61)–(64) should be suppressed by the factor $\sim\epsilon^2$. We show now by numerical analysis that the correlation functions (61)–(64) indeed behave in a way very similar to the correlation functions (48)–(50) with odd r. In Fig. 23, we show the r dependence of the correlation functions (61)–(64) in a system of length $L = 400$. We observe that in the critical regime of not too large r (the condition is $r \ll \xi_\epsilon$) the function $C_{F,1,o}$ dominates. It is also seen that the magnitude of this term is quite small. To understand the source of this smallness and its parametric dependence, we show in Fig. 24 the dependence of the correlation functions on system size L and on the energy ϵ. The right panel clearly shows the ϵ^2 scaling that is expected from the analytical argument and is fully analogous to the scaling in Fig. 21. This is translated into an exponential scaling with respect to $\sqrt{L}$ of correlation

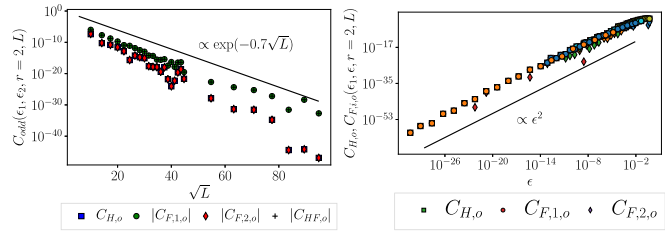

FIG. 24. (Left) Scaling of the correlation functions $C_{H,o}(\epsilon_1, \epsilon_2, r = 2, L)$, $C_{F,1,o}(\epsilon_1, \epsilon_2, r = 2, L)$, $C_{F,2,o}(\epsilon_1, \epsilon_2, r = 2, L)$, and $C_{HF,o}(\epsilon_1, \epsilon_2, r = 2, L)$, Eqs. (61)–(64) with respect to system size L. (Right) Scaling of the same correlation functions with energy. Different colors represent L from 100 to 10 000. The data clearly demonstrated the ϵ^2 scaling that is also expected analytically.

functions evaluated on two lowest-energy states, as is seen in the left panel of Fig. 24 and is again in full analogy with the corresponding behavior in Fig. 21.

The ϵ^2 scaling of the correlation functions (61)–(64) implies the RG irrelevance of the corresponding interaction term. Indeed, the density of states increases only as $1/\epsilon$ with logarithmic correction, see Eq. (34), and thus the suppression of the interaction wins over the increase of the density of states. We will verify this numerically below (Fig. 27). As explained above, the reason behind the ϵ^2 suppression of the matrix elements is the fact that both even and odd sites are involved. This tells us which correlation functions may escape such a suppression: those that involve sites of one sublattice only, i.e., with all distances between the sites being even. We thus consider such a generalized interaction term:

$$\hat{O} = \gamma_k \gamma_{k+2} \gamma_{k+r} \gamma_{k+r+2}, \tag{65}$$

with an even $r \geqslant 4$. Such a term is allowed by symmetries and will be generalized by RG from the original interaction. This leads us to introduce the corresponding generalization of the correlation functions (61)–(64):

$$C_{H,e}(\epsilon_\alpha, \epsilon_\beta, r, L) = \langle U_{k,\alpha} U_{k+2,\alpha} U_{k+r,\beta} U_{k+r+2,\beta} \rangle_{\rm dis}, \tag{66}$$

$$C_{F,1,e}(\epsilon_\alpha, \epsilon_\beta, r, L) = \langle U_{k,\alpha} U_{k+2,\beta} U_{k+r,\alpha} U_{k+r+2,\beta} \rangle_{\rm dis}, \tag{67}$$

$$C_{F,2,e}(\epsilon_\alpha, \epsilon_\beta, r, L) = \langle U_{k,\alpha} U_{k+2,\beta} U_{k+r,\beta} U_{k+r+2,\alpha} \rangle_{\rm dis}, \tag{68}$$

$$\begin{aligned} C_{HF,e}(\epsilon_\alpha, \epsilon_\beta, r, L) = &\langle U_{k,\alpha} U_{k+2,\alpha} U_{k+r,\beta} U_{k+r+2,\beta} \\ &+ U_{k,\alpha} U_{k+2,\beta} U_{k+r,\alpha} U_{k+r+2,\beta} \\ &- U_{k,\alpha} U_{k+2,\beta} U_{k+r,\beta} U_{k+r+2,\alpha} \rangle_{\rm dis}. \end{aligned} \tag{69}$$

The subscript "e" indicates that all distances between the sites involved are even, in analogy with correlation functions (48)–(50) at even r.

In view of the analogy that we have just emphasized, we can expect that (i) the correlation function $C_{H,e}$ scales similarly to C_H, (48), and (ii) the correlation functions $C_{F,1,e}$ and $C_{F,2,e}$ scale in the same way and, moreover, are equal in the leading order to $C_{H,e}$, in analogy with the corresponding behavior of C_F, (49). However, since we now have three terms rather than two, the strong Hartree-Fock compensation should

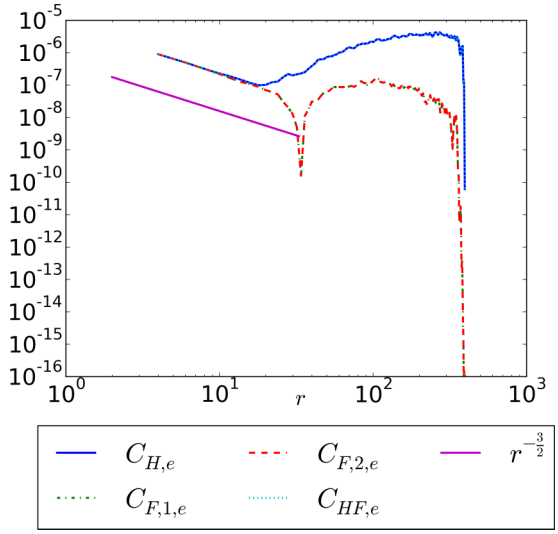

FIG. 25. Correlation functions $C_{H,e}(\epsilon_1, \epsilon_2, r, L = 400)$, $C_{F,1,e}(\epsilon_1, \epsilon_2, r, L = 400)$, $C_{F,2,e}(\epsilon_1, \epsilon_2, r, L = 400)$, and $C_{HF,e}(\epsilon_1, \epsilon_2, r, L = 400)$ evaluated on two lowest-energy eigenstates, as functions of even r. The functions $C_{H,e}$, $C_{F,1,e}$, and $C_{F,2,e}$ are nearly equal to each other and scale as $r^{-3/2}$. In $C_{HF,e}$, two out of three terms approximately cancel, leaving $C_{HF,e} \simeq C_{H,e}$.

not happen, leaving us with $C_{HF,e} \simeq C_{H,e}$. These expectation are fully supported by the numerical simulations. In Fig. 25, we show the r dependence of the correlation functions (66)–(69) evaluated on two lowest-energy eigenstates in a system of size $L = 400$. All four correlations functions $C_{H,e}$, $C_{F,1,e}$, $C_{F,2,e}$, and $C_{HF,e}$ are nearly equal in the critical regime (not too large r) and show the $r^{-3/2}$ scaling in analogy with C_H and C_F. In fact, the overall behavior of the correlation function $C_{H,e}$ ($C_{F,1,e}$ and $C_{F,2,e}$) in Fig. 25 is remarkably similar to that of C_H (respectively, C_F) in Fig. 19. We turn now to the scaling of the correlation functions (66)–(69) with energy ϵ and length L, see Fig. 26. The figure is very similar to the upper two panels of Fig. 20 and confirms that $C_{H,e}$, $C_{F,1,e}$, and $C_{F,2,e}$ scale exactly in the same as C_H with even r, (56). Since the Hartree-Fock compensation is not operative now, the correlation function $C_{HF,e}$ scales in the same way.

Since the correlation function $C_{HF,e}$ decreases with L in a power-law fashion only, and the density of states increases in an exponential way, they product should clearly increase

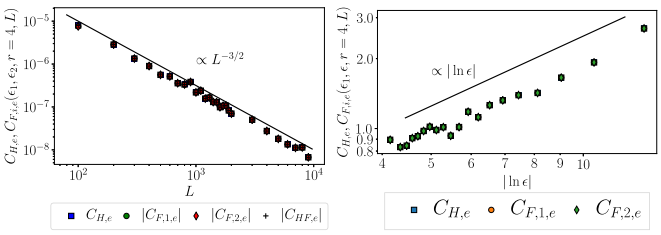

FIG. 26. Correlation functions (66)–(69) with $r = 4$. (Left) Scaling with the system size L of the correlation functions evaluated on two lowest-energy eigenstates. The slope corresponds to a power law with an exponent 3/2. (Right) Dependence on energy at fixed $L = 4000$. The slope corresponds to the $|\ln\epsilon|$ scaling. The total scaling with L and ϵ is therefore the same as for the complex-fermion correlation function C_H with even r, Eq. (56).

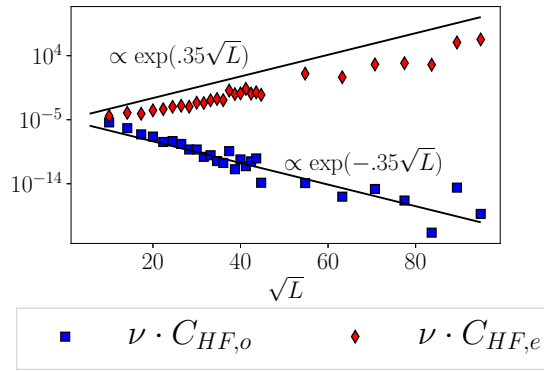

FIG. 27. RG (ir)relevance of interaction at the infinite-randomness fixed point of the majorana chain. Product $\nu(L)C_{HF,\{e,o\}}(\epsilon_1, \epsilon_2, r, L)$ of the Hartree-Fock correlation function and the density of states is plotted vs the system size L. Blue symbols: $\nu C_{HF,o}$ for $r = 2$ quickly decreases with L, implying RG irrelevance of the corresponding interaction terms. Red symbols: $\nu C_{HF,e}$ for $r = 4$ quickly increases with L, indicating RG relevance of the corresponding interaction term.

exponentially. This is explicitly demonstrated in Fig. 27. For comparison, we also show there the product $\nu C_{HF,e}$ that decreases with increasing L as discussed above. The exponential increase of $\nu C_{HF,e}$ indicates the RG relevance of the corresponding interaction term. This explains why the interaction drives the system away from the infinite-randomness fixed point and establishes the spontaneous symmetry breaking and localization, as exhibited by the DMRG results, Sec. III B.

At this point, the following comment is in order. The completeness of eigenstates in combination with the chiral symmetry implies that $\sum_{\epsilon_\alpha > 0} U_{k,\alpha} U_{k+r,\alpha}$ is equal to zero for any even $r \neq 0$. As a result, the correlation functions (66)–(69) are zero when summed over all states with positive energies. Exactly such sums will arise if we calculate the expectation of the interaction (65) over the vacuum state (or, more generally, over any Fock-space basis state). However, what we are actually interested in is not this expectation value but rather the effect of nondiagonal matrix elements of the interaction. In more conventional problems, it turns out that it is sufficient to study the scaling of the expectation value to understand the effect of the interaction. It turns out that the situation with the term of the type (65) in the present problem is more delicate. The full analysis of the effect of nondiagonal matrix elements of such an interaction at the infinite-randomness fixed point is a very challenging task that we leave to future work. We expect that two properties of the correlation functions (66)–(69) that we have identified above—namely, (i) the contributions that, when multiplied with the density of states, strongly increase with L and (ii) the absence of Hartree-Fock cancellation of such contributions—will be also key ingredients of such a more sophisticated analysis, thus governing the RG relevance of the interaction for the disordered Majorana chain.

VI. SUMMARY AND OUTLOOK

The main goal of this work was the investigation of the low-energy physics of a chain of Majorana fermions in

the presence of interaction and disorder. One of intriguing questions was a difference between this interacting Majorana problem and the 1D model of interacting complex fermions with chiral symmetry that belongs to the same symmetry class BDI. In the absence of interaction, both models are equivalent (apart from halving the number of states in the Majorana case), and flow into the same infinite-randomness fixed point. It turns out that the interaction makes them drastically different. To explore and understand the physics of these models, we have used a combination of several computational and analytical approaches, including DMRG, mean-field analysis, and two different types of RG (around the clean interacting fixed point and around the noninteracting disordered fixed point). The latter type of RG required investigation of statistical properties of eigenfunction correlations at infinite-randomness fixed point, which has turned out to be a very interesting and nontrivial problem by itself. Our key results can be summarized as follows:

(1) We have carried out the DMRG analysis of the models (in their spin representations), by calculating the entanglement entropy as well as the spin-spin correlation functions. This has allowed us to determine the corresponding phase diagrams and to understand some physical properties of the emerging phases. More specifically:

(i) we have first considered an interacting Majorana chain with staggering, see Figs. 3 and 4 for the color-code representation of the entanglement entropy and the spin correlations in the interaction-staggering plane. The obtained phase diagram is shown in Fig. 5. On the no-staggering (self-dual) line, we observe the Ising (central charge $c = 1/2$) and Ising + LL ($c = 3/2$) phases, in agreement with Ref. [26]. Away from the self-dual line (i.e., in the presence of staggering), we find gapped phases as well as a LL critical phase with $c = 1$. The distinct character of phases manifests itself in the spatial dependence of the spin-spin correlation functions, Fig. 6. The $c = 1$ critical phase can be understood as the result of gapping the Ising sector of the LL + Ising phase, with LL sector remaining gapless. The gapped phases on both side of the self-dual line are topologically distinct. We have also found interesting parts of the gapped phases with entanglement entropy showing relatively sharp maxima at points where the antiferromagnetic ordering of spins experience certain "phase slips."

(ii) We have then applied the DMRG analysis to interacting disordered Majorana chains. Here we focused on the systems without staggering, which are critical in the absence of disorder. In the case of attractive interaction, our DMRG results on entanglement show that the system remains critical also in the presence of disorder. Moreover, as shown in Fig. 7, we find (within the numerical accuracy) the same value of the central charge, $c = 1/2$, as for the clean system. The situation is radically different for the repulsive interaction, where we find that the system gets localized. This happens already for weak repulsion (for which the clean system hat $c = 1/2$ central charge), as is seen from the behavior of the entanglement entropy, Fig. 8. The behavior of the spin correlation function, Fig. 9, demonstrates that the system finds itself spontaneously in one of two topological phases. A similar behavior is observed for the intermediate strength of the interaction, Figs. 10 and 11. Thus an interplay of repulsive disorder and interaction leads to a spontaneous symmetry breaking that results in localization and topological ordering.

(iii) In the case of disordered interacting complex fermions, the DMRG shows (both in the cases of attraction and repulsion) the same behavior as for the noninteracting model. Specifically, the found value of the central charge is $c = \ln 2$, Fig. 12, which is a hallmark of the infinite-randomness fixed point.

(2) As a first attempt to add analytical understanding to the numerical results, we have developed a weak-disorder RG in spirit of Giamarchi-Schulz. This was done in the vicinity of all three clean critical theories: $c = 1/2$ and $3/2$ for Majorana chain and $c = 1$ for complex fermions. In all the cases, the disorder is RG-relevant and drive the system away from the corresponding clean fixed point, towards the strong-disorder regime. Therefore this approach is not sufficient for exploring the infrared behavior of the models.

(3) The flow of disorder to strong coupling has motivated an alternative RG analysis, in which the starting point is the noninteracting disordered theory that is at the strong-randomness fixed point. Investigation of the effect of interaction requires understanding of the scaling of eigenfunction correlations at this fixed point. This theory is a remarkable strong-disorder Anderson-localization critical theory, and the corresponding eigenfunction statistics is also highly interesting on its own, so that we have studied it in some detail. For the Hartree-type correlations of two eigenfunctions at even distance r, we have determined, by combination of numerical and analytical means, the critical scaling (56). This formula shows that, in analogy with Anderson-transition critical points in higher dimensions, correlations are strongly enhanced at criticality (small ϵ) and at small r. On the other hand, for odd r, the correlations turn out to be strongly suppressed at criticality, in view of the chiral symmetry. Furthermore, we show that a strong cancellation between the Hartree and Fock terms leads to a strong suppression of Hartree-Fock correlation function also for even r. We have shown that this suppression overweights the divergence of the density of states at criticality, Fig. 22. As a result, the interaction turns out to be RG-irrelevant at the strong-disorder fixed point for the complex-fermion model, in full consistency with the corresponding DMRG results.

For Majorana problem, the interaction matrix elements involves four sites. For even separation between the sites, the critical scaling of the corresponding eigenstate correlation functions, Fig. 25, is analogous to that of two-point correlation function C_H, Eq. (56). The crucial difference is that in the Majorana case, for given two eigenstates and a give set of spatial points there are three contributing correlations functions instead of two (Hartree and Fock) in the complex-fermion case. As a result, the Hartree-Fock cancellation is not operative in the Majorana problem, and the interaction is relevant at the infinite-randomness fixed point. This is again consistent with the DMRG results and explains a dramatic difference between the behavior of interacting disordered Majorana chains and that of its complex-fermion counterpart.

Before closing the paper, we make several comments on possible extensions of our work that represent prospective directions for future research.

(i) It would be interesting to extend our analysis of disordered interacting Majorana systems to higher-dimensional systems including quasi-1D (ladders) and 2D geometry. Clean version of such models was studied in Ref. [63].

(ii) Another potential extension concerns the symmetry class. We recall that the Majorana model that we have considered in this paper belongs to the symmetry class BDI. If the sublattice symmetry is violated, the system will be in the symmetry class D. It would be interesting to study the interacting Majorana models of this symmetry class in 1D, quasi-1D, and 2D geometries. In particular, an intriguing question is how generic is the difference between interacting Majorana and complex-fermion models from the same symmetry class.

(iii) Our numerics show that the behavior of the disordered Majorana chain differs strongly for attractive and repulsive interaction. Specifically, we find localization in the repulsive case, whereas the system remains critical for attractive g, see right panel of Fig. 7. Analytical understanding of the impact of the sign of the interaction would be desirable. Further, the physics of the disordered attractive interaction case itself deserves a more detailed study. The numerical data suggest the value $c = 1/2$ of the central charge, different from the value $c = (\ln 2)/2$ characterizing the noninteracting system. This difference is consistent with our finding that the interaction in Majorana chain is relevant at the infinite-randomness fixed point of the noninteracting system. On the other hand, we also know that the disorder is relevant at the clean fixed point, so that the coincidence of the found central charge with that of the clean system appears surprising. Further investigation of other physical observables should help to clarify the precise physical nature of this phase.

(iv) The spontaneous symmetry breaking in disordered interacting Majorana chains, which leads to localization and topological order, calls to exploring the physics of these systems at high temperatures. It is expected that they will undergo a many-body (de-)localization transition accompanied by restoration of symmetry. Transitions between many-body localized and ergodic phases have attracted a great deal of attention in recent years [64–67].

(v) A complete analysis of statistical properties of various eigenfunction correlations (also those including a larger number of eigenstates and/or spatial points) at the infinite-randomness fixed point represents a very interesting (and also very challenging) problem. This fixed point represents an intriguing example of a strong-disorder Anderson-localization critical theory. In fact, it was argued in Ref. [68] that a "superuniversality" holds in the sense that the same fixed point describes critical theories of all five symmetry classes (BDI, AIII, CII, D, DIII) that can host 1D topological insulators according to the "periodic table." This fixed point exhibits criticality in various observables, but at the same time many properties are similar to those in the localized phase. In this respect, this noninteracting 1D critical point bears a certain similarity with the transition between the localized and ergodic phases on random regular graphs [69] that serves as a toy model for the many-body localization transition.

(vi) Another interesting generalization of our models is including disorder in the interaction terms. For relatively weak randomness of the interaction, the results derived here are expected to retain validity, since such terms are generated anyway during RG flow. On the other hand, if the random interaction is a dominant part of the Hamiltonian, the models will resemble those of Sachdev-Ye-Kitaev (SYK) type [70]. The scenario of not fully quenched kinetic energy is considered in Refs. [71,72], where coupled quantum dots are studied. It would be interesting to see whether the SYK-like physics may emerge in our model in the case of strong random interaction. In this case, one could study a crossover between the SYK and the infinite-randomness fixed point.

ACKNOWLEDGMENTS

We gratefully acknowledge collaboration with N. Kainaris at the early stage of this work. We also thank E. Doggen and K. S. Tikhonov for help with numerical simulations and M. Foster for discussions and for sharing his unpublished notes on 1D chiral-class models. The work was supported by the Deutsche Forschungsgemeinschaft via the Grant No. MI 658/7-2 (Priority Programme 1666 "Topological Insulators").

APPENDIX A: WEAK-DISORDER RG AROUND THE ISING + LL FIXED POINT OF THE INTERACTING MAJORANA CHAIN

In this Appendix, we provide details of the weak-disorder RG treatment of the interacting Majorana chain in the Ising + LL fixed point, Sec. IV C. The starting point is the effective mean-field Hamiltonian (25) including the third-nearest-neighbor hopping as well as a weak randomness in the nearest-neighbor hopping $t + \delta t_j$, supplemented with the interaction term $g\gamma_j\gamma_{j+1}\gamma_{j+2}\gamma_{j+3}$.

Using the low-energy expansion (26) for the nearest-neighbor hopping operator $\gamma_j\gamma_{j+1}$ yields oscillatory contributions with wave vectors $k_i = 0$, k_0, $k_0 + \pi$, $2k_0$, $2k_0 + \pi$, and π that can be dropped in the clean case. In the presence of randomness, they couple, however, to the corresponding Fourier harmonics of disorder δt_j. We employ the replica trick to average over disorder. As a result, the following terms in the action representing effective "interactions" between different replica species a and b are generated:

$$S_{k_0} = -\frac{8(1-\cos k_0)}{\pi a} D_{k_0} \int dx d\tau d\tau' \sum_{a,b} \big[i\gamma_L^a \gamma_L^b \sin(\phi_a + \theta_a - \phi_b - \theta_b)$$
$$+ i\gamma_R^a \gamma_R^b \sin(\phi_a - \theta_a - \phi_b + \theta_b) - i\gamma_L^a \gamma_R^b \sin(\phi_a + \theta_a - \phi_b + \theta_b) \big],$$
$$S_{k_0+\pi} = -\frac{8(1+\cos k_0)}{\pi a} D_{k_0+\pi} \int dx d\tau d\tau' \sum_{a,b} \big[i\gamma_L^a \gamma_L^b \sin(\phi_a - \theta_a - \phi_b + \theta_b)$$

$$+ i\gamma_R^a\gamma_R^b \sin(\phi_a + \theta_a - \phi_b - \theta_b) - i\gamma_L^a\gamma_R^b \sin(\phi_a - \theta_a - \phi_b - \theta_b)\big],$$

$$S_{2k_0} = -\frac{1}{\pi^2 a^2} D_{2k_0} \int dx d\tau d\tau' \sum_{a,b} \cos(2\phi_a - 2\phi_b)\sin(2\theta_a)\sin(2\theta_b),$$

$$S_{2k_0+\pi} = -\frac{1}{(\pi a)^2} D_{2k_0+\pi} \int dx d\tau d\tau' \sum_{a,b} \cos(2\phi_a - 2\phi_b),$$

$$S_{\pi} = -\frac{8}{\pi a} D_{\pi} \int dx d\tau d\tau' \sum_{a,b} \big[4\gamma_L^a\gamma_R^a\gamma_R^b\gamma_L^b + \cos^2 k_0 \cos(2\theta_a)\cos(2\theta_b)\big]. \tag{A1}$$

Each term S_{k_i} is labeled by the corresponding momentum component k_i. Some of the terms allow for a simple physical explanation. In particular, the action term $S_{2k_0+\pi}$ represents the backscattering between the right and left Fermi points of the emergent Luttinger-liquid sector, while S_π corresponds to backscattering processes commensurate with the lattice. The RG equations summarized in Table I and Eq. (28) are then inferred in analogy with Ref. [51]. The most relevant terms are $S_{2k_0+\pi}$ and S_π. The contribution of the term $S_{2k_0+\pi}$ to the renormalization of K, Eq. (28), is analogous to backscattering in Giamarchi-Schulz RG. For the other term, S_π, the duality exchanging $\phi \leftrightarrow \theta$ and $K \leftrightarrow K^{-1}$ may be used to find the contribution to K.

While the forward scattering can be completely gauged away in the standard Giamarchi-Schulz RG, here the transformation gauging it out generated additional terms. However, a direct inspection shows that they are irrelevant in the RG sense.

The interaction generates a replica-diagonal term that couples the Luttinger-liquid and Majorana sectors:

$$S_{\rm int} = -g' \int dx d\tau \sum_a \gamma_L^a\gamma_R^a(\Psi_L\Psi_R + \Psi_L^\dagger\Psi_R^\dagger)$$

$$= -2g' \int dx d\tau \sum_a \gamma_L^a\gamma_R^a \cos(2\theta_a). \tag{A2}$$

This term is RG-irrelevant in the range of interest, $K < 1$; the corresponding dimensional coupling is denoted y' in Table I. Higher terms respecting the symmetry are, of course, also generated. It can be checked by dimension counting that all terms arising due to interaction remain irrelevant in the range $1/4 < K < 1$.

APPENDIX B: ORIGIN OF LOW-ENERGY SUPPRESSION OF WAVE FUNCTION CORRELATIONS IN DISORDERED COMPLEX-FERMION CHAIN

In this Appendix, we present analytical arguments explaining the origin of the suppression of eigenstate correlations in a complex-fermion chain at low energies found numerically in Sec. V B. An eigenvector $U_{i+1,\epsilon}$ of Hamiltonian (39) fulfills the following transfer matrix equation:

$$\begin{pmatrix} U_{i+1,\epsilon} \\ U_{i,\epsilon} \end{pmatrix} = \begin{pmatrix} \epsilon/t_{i+1} & -t_i/t_{i+1} \\ 0 & 1 \end{pmatrix} \begin{pmatrix} U_{i,\epsilon} \\ U_{i-1,\epsilon} \end{pmatrix}. \tag{B1}$$

For zero energy, $\epsilon = 0$, two sublattices are decoupled, so that the wave function lives on one sublattice. For finite (but small), ϵ the wave function on the second sublattice is suppressed by ϵ. This implies the suppression of the correlation functions $C_2(\epsilon, r, L)$, $C_H(\epsilon_\alpha, \epsilon_\beta, r, L)$, and $C_F(\epsilon_\alpha, \epsilon_\beta, r, L)$ for odd r by a factor $\sim\epsilon_>^2$, where $\epsilon_>$ is the larger of two energies $\epsilon_\alpha, \epsilon_\beta$. This suppression is indeed numerically observed, see Fig. 16 and the right panel of Fig. 21 which make evident the $\epsilon_>^2$ scaling of the odd-r correlation functions. As is seen in this figure, for odd r, the Fock term is substantially smaller than the Hartree one, so that there is no cancellation between them and $C_{\rm HF} \simeq C_H$.

For even r, an even stronger suppression holds for the Hartree-Fock correlation function. As an example, consider $r = 2$. Using the transfer-matrix equation (B1), we get the relation

$$\begin{aligned} &|U_{i,\epsilon_\alpha}|^2|U_{i+2,\epsilon_\beta}|^2 + |U_{i+2,\epsilon_\alpha}|^2|U_{i,\epsilon_\beta}|^2 \\ &\quad - 2U_{i,\epsilon_\alpha}U_{i+2,\epsilon_\alpha}U_{i+2,\epsilon_\beta}U_{i,\epsilon_\beta} \\ &= \frac{1}{t_{2+i}^2}\big(\epsilon_\alpha^2|U_{i+1,\epsilon_\alpha}|^2|U_{i,\epsilon_\beta}|^2 \\ &\quad - 2\epsilon_\alpha\epsilon_\beta U_{i,\epsilon_\alpha}U_{i+1,\epsilon_\alpha}U_{i+1,\epsilon_\beta}U_{i,\epsilon_\beta} + \epsilon_\beta^2|U_{i,\epsilon_\alpha}|^2|U_{i+1,\epsilon_\beta}|^2\big). \end{aligned} \tag{B2}$$

The left-hand side of Eq. (B2) is the difference between the Hartree and Fock terms that enters the correlation function $C_{\rm HF}$ for $r = 2$. On the other hand, the right-hand side is the linear combination of C_H and C_F terms for $r = 1$, each of them multiplied by a factor quadratic in energies. We have thus proven that $C_{\rm HF}$ for $r = 2$ is suppressed by an additional factor $\sim \epsilon_>^2$ in comparison with the $r = 1$ correlation function $C_{\rm HF} \simeq C_H$,

$$C_{\rm HF}(\epsilon_\alpha, \epsilon_\beta, 2, L) \sim \epsilon_>^2 C_{\rm HF}(\epsilon_\alpha, \epsilon_\beta, 1, L). \tag{B3}$$

The same argument holds for other even r. This is fully supported by the numerical data, as shown in Fig. 28 where we plot the ratio $C_{\rm HF}(\epsilon_1, \epsilon_n, 2, L)/C_{\rm HF}(\epsilon_1, \epsilon_n, 1, L)$ multiplied by ϵ_n^{-2} for different n, as a function of L. We remind the reader that ϵ_n scales exponentially as a function of L and n, see Eq. (36). Each of the factors $C_{\rm HF}(\epsilon_1, \epsilon_n, 2, L)$, $C_{\rm HF}(\epsilon_1, \epsilon_n, 1, L)$, and ϵ_n^{-2}, when taken separately, changes within an enormous range of many dozens of decades, see, e.g., Figs. 20 and 21. On the other hand, the product plotted in Fig. 28 changes only weakly (at most linearly in L, which means logarithmically in ϵ), in full agreement with the analytical argument.

Since we have shown above that the odd-r correlation function in the right-hand side of Eq. (B3) scales as $\epsilon_>^2$, the

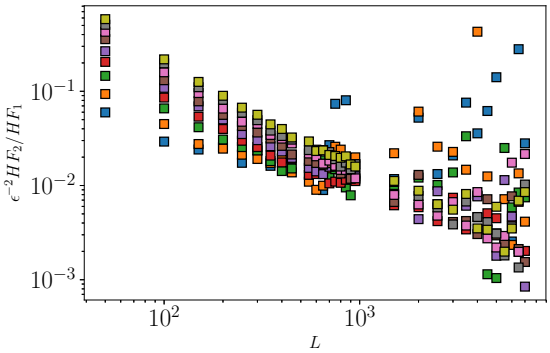

FIG. 28. Ratio $C_{\rm HF}(\epsilon_1, \epsilon_n, 2, L)/C_{\rm HF}(\epsilon_1, \epsilon_n, 1, L)$ multiplied by ϵ_n^{-2} for the first twenty levels n (in distinct colors) as a function of L. The data show only a weak (at most linear) dependence on L (that corresponds to a logarithmic energy dependence), which should be contrasted to the exponential L dependence of both entering correlation functions $C_{\rm HF}$ and of the energy ϵ_n. This confirms the analytic prediction in Eq. (B3), with possible logarithmic-in-energy corrections.

even-r Hartree-Fock correlator should scale as $\epsilon_>^4$ according to this equation. The $\epsilon_>^4$ scaling of $C_{\rm HF}$ for even r is indeed observed numerically, see Fig. 20.

APPENDIX C: DISORDERED MAJORANA CHAIN WITH MEAN-FIELD TREATMENT OF INTERACTION IN THE ISING + LL PHASE

In this Appendix, we present an analysis of the disordered Majorana chain that treats disorder exactly and the interaction on the mean-field level. This approach is in a sense complementary to those in the main text of the paper. In the weak-disorder RG of Sec. IV, the interaction was treated exactly and the disorder was considered as a perturbation. Contrary to this, the analysis of Sec. V considered disorder exactly and the interaction perturbatively. Here, we treat the disorder by using the field-theoretical σ model approach. This treatment is essentially exact, in analogy with Sec. V. The key differences with Sec. V are that (i) we consider a sufficiently strong repulsive interaction for which the clean system is in the Ising + LL phase, and (ii) we include the interaction on the mean-field level only. This allows us to obtain the phase diagram of the system in the plane spanned by the disorder strength and the staggering. The phase diagram contains four distinct topological phases. Of course, we know from Sec. V and from the numerical study in Sec. III B that including effects of interaction beyond the mean-field level destabilizes the system on the critical line. This means that the transitions between the topological phases are in fact not of second order (as found in the mean-field treatment below) but rather of first order. On the other hand, the phase diagram is expected to remain applicable also beyond the mean-field level.

At a mean-field level with respect to the interaction, the third-nearest-neighbor hoppings are generated and the nearest-neighbor hopping is renormalized. The full mean-field Hamiltonian, including the randomness δt_j in the nearest-neighbor hopping, reads

$$H_{I+LL}^{\rm MF} = \frac{i}{2}\sum_j [(t_1 + t_2 + (-1)^j(t_1 - t_2) + 2\delta t_j)\gamma_j\gamma_{j+1} + ((t_1' + t_2') + (-1)^j(t_1' - t_2'))\gamma_j\gamma_{j+3}]. \quad \text{(C1)}$$

By choosing $t_1 \neq t_2$ or $t_1' \neq t_2'$, the system can be staggered. The random component δt_j of the hopping is assumed to have Gaussian statistics, with zero average.

The formalism presented in Refs. [73,74] for a particular model can be extended to the case of generic banded Hamiltonians. For convenience, we have performed computations in class AIII instead of BDI (i.e., allowing for complex δt_j). The results for AIII shown here remain essentially the same for the class BDI as can be checked numerically using transfer matrices.

The calculations proceed by integrating out the disorder using the supersymmetry formalism. After Hubbard-Stratonovich decomposition and saddle-point expansion (which yields the self-consistent Born approximation), one arrives at a nonlinear sigma model describing the disordered wire. The action describes the soft modes $T \in {\rm GL}(1|1)$:

$$S[T] = \tilde{\chi}\,{\rm str}(T\partial T^{-1}) - \frac{\tilde{\xi}^2}{4}{\rm str}(T\partial^2 T^{-1}). \quad \text{(C2)}$$

There are two coupling constants here: $\tilde{\xi}$ has a meaning of the bare conductance, and $\tilde{\chi}$ of the bare topological index. Under RG, these coupling constants get renormalized. The theory thus exhibits a two-parameter RG flow, which is largely analogous to the Khmelnitskii-Pruisken flow for the 2D theory describing the quantum Hall effect.

Except for the case of half-integer bare values, $\tilde{\chi}$ flows to the nearest integer value, which is the actual topological index χ. Half-integer values of $\tilde{\chi}$ are stable under RG-flow and correspond to critical theories at the boundary of two topologically distinct phases. To determine the phase diagram, one thus should compute the dependence of the bare index $\tilde{\chi}$ on parameters of the chain. These dependencies are obtained when one derives the σ model from the microscopic model, as sketched above. We skip details of this calculation, since it is analogous to that carried out for a different microscopic model in Ref. [74]. A general 1D noninteracting Hamiltonian H with chiral symmetry and with translational invariance in average can be written as

$$H = h_n\sum_i a_{i+n}^\dagger b_i + \sum_i r_{n,i}a_{i+n}^\dagger b_i + {\rm H.c.} \quad \text{(C3)}$$

Here, a_i and b_i are operators on two sublattices, h_n are the average hopping matrix elements, and $r_{n,i}$ are random contributions to hopping that are characterized by zero mean and by the variance

$$\langle r_{n,i}r_{m,j}^*\rangle = w_n\delta_{i,j}\delta_{n,m}. \quad \text{(C4)}$$

We find the following result for the bare index $\tilde{\chi}$ in terms of the parameters of H:

$$\tilde{\chi} = \sum_q \frac{h^-(q)v^+(q)}{\Sigma_0^2 + h^+(q)h^-(q)} + \sum_n nu_n, \quad \text{(C5)}$$

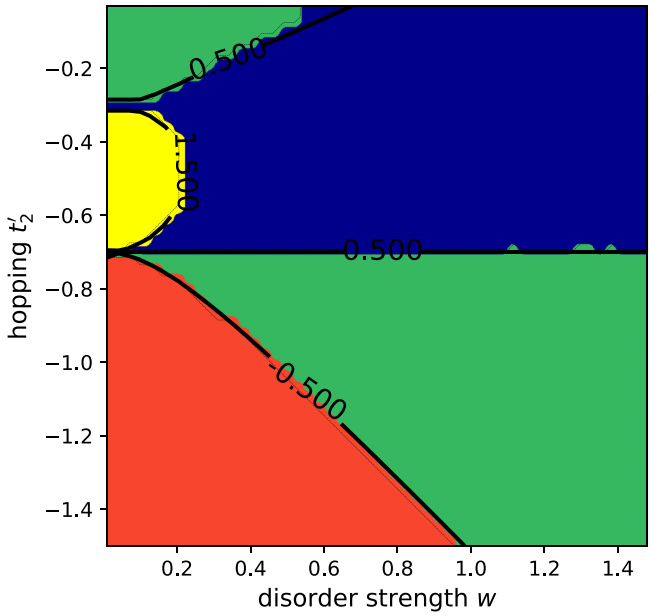

FIG. 29. Phase diagram of the mean-field Hamiltonian (C1) describing the Ising + LL phase of the disordered Majorana chain. The parameters $t_1' = -0.7$ and $t_2 = t_1 = t = 1$ are fixed. The phase diagram is shown in the plane spanned by disorder w and the hopping t_2'. The zero staggering corresponds to $t_2' = t_1' = -0.7$. Black lines are phase boundaries as obtained analytically via mapping on the σ model from the condition that the bare index $\tilde{\chi}$ is half-integer. Colored regions are four distinct topological phases with the values of the topological index χ equal to -1 (red), 0 (green), 1 (blue), and 2 (yellow), as obtained from the transfer-matrix numerics. A perfect agreement between numerical and analytical results is observed. At zero disorder, $w = 0$, and zero staggering, $t_1' - t_2' = 0$, three critical lines meet, yielding a critical theory with central charge $c = 3/2$.

where

$$h^-(q) = \sum_n h_n e^{-inq}, \tag{C6}$$

$$h^+(q) = \sum_n h_n e^{inq}, \tag{C7}$$

$$v^+(q) = \sum_{m,n} (n-m) u_n h_m e^{imq}, \tag{C8}$$

$$u_n = \frac{w_n^2}{\sum_m w_m^2}, \tag{C9}$$

and the self-energy Σ_0 is a solution of the equation

$$\left(\sum_n w_n^2\right) \sum_q \frac{1}{\Sigma_0^2 - h^+(q)h^-(q)} = 1 \tag{C10}$$

representing the self-consistent Born approximation.

Our Hamiltonian (C1) is a particular case of Eq. (C3). The nearest- and third-nearest-neighbor hopping of Eq. (C1) are encoded in terms of Eq. (C3) in $h_1 = t_1$, $h_2 = t_1'$, $h_0 = t_2$, and $h_{-1} = t_2'$. Further, the randomness in the nearest-neighbor hopping of Eq. (C1) translates into $u_0 = 1/2$ and $u_1 = 1/2$. The resulting phase diagram in the parameter plane spanned by disorder strength w and staggering $t_1' - t_2'$ is shown in Fig. 29.

We have compared the analytical results (black lines show the corresponding phase boundaries in Fig. 29) with those of direct transfer matrix numerics. Four topological phases(with $\chi = -1$, 0, 1, and 2) as obtained by the latter approach are shown by different colors in Fig. 29. An excellent agreement between the analytical and numerical data is observed. This is quite nontrivial since (i) the σ model derivation holds in the limit of large number of channels, $N \gg 1$, whereas our model corresponds to $N = 3$, (ii) the analytical calculation of parameters of the σ model is controlled fir weak disorder, $w/t \ll 1$, whereas we find a very good agreement also for $w/t \sim 1$.

The self-duality transformation ensures that the zero-staggering line ($t_2' = -0.7$ in Fig. 29) is critical within this mean-field analysis. An important observation is that the critical line is adjacent only to 0 (green) and 1 (blue) topological phases for finite disorder.

In the clean DMRG analysis, Sec. III A, only two distinct topological phases were observed, which correspond to the green and blue phases of Fig. 29. The other two phases (red and yellow) can only be reached by adding the third-nearest-neighbor hopping explicitly [26] since otherwise the Hamiltonian (C1) with the corresponding parameters can not be obtained as a mean-field Hamiltonian of an interacting Majorana chain. When disorder is added to the mean-field model, we observe that the parameter space for the red and yellow phases shrinks.

APPENDIX D: ANALYTICAL APPROACH TO WAVE FUNCTION CORRELATIONS

In this Appendix, we provide analytical results for the scaling of eigenfunction correlation functions at the infinite-randomness fixed point. These results complement, support, and explain the corresponding numerical results in Sec. V.

In Ref. [36], the average of one Green's function in a noninteracting 1D model of class BDI was computed by means of supersymmetry formalism that allowed to map the problem onto quantum mechanics of a SU(1|1) spin. In order to obtain directly the correlation functions of two eigenstates, one would need to average products of two Green's functions with the corresponding energy and spatial arguments. While the mapping on a supersymmetric quantum mechanics can be generalized to this situation, the solution of the corresponding problem becomes extremely difficult. For this reason, we choose below a slightly different approach and calculate, by using the supersymmetry technique, the averaged square of the Green's function at an imaginary frequency. This average is related, by virtue of a spectral decomposition, to the two-eigenstate correlation functions. The resulting conclusions on the scaling of the two-eigenstate correlations are in agreement with our numerical findings in Sec. V.

We follow the formalism of Ref. [36] and map the original lattice model with random hopping onto a continuous model of a Dirac fermion with random mass, cf. Sec. IV A. The latter is considered to be delta-correlated and Gaussian-distributed disorder, with the strength W (which sets the ultraviolet cutoff for the critical theory and can be set to unity). Within the mapping onto the supersymmetric quantum mechanics, the averaged Green's function at an imaginary frequency $i\omega$ and

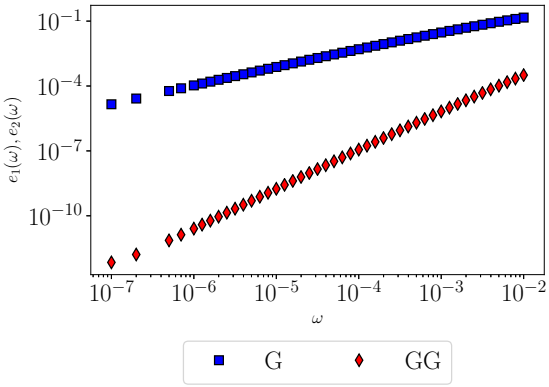

FIG. 30. In this plot, the validity of Eqs. (D1) and (D2) for $\langle G(i\omega)\rangle_{\rm dis}$ and $\langle G(i\omega)G(i\omega)\rangle_{\rm dis}$ derived in a continuum-limit approximation to the effective Schrödinger equation is verified numerically. For this purpose, we plot $e_1(\omega) = i\omega\langle G(i\omega)\rangle_{\rm dis} - |\ln(\omega/a_0)|^{-2}$ and $e_2(\omega) = 3\omega^2\langle G(i\omega)G(i\omega)\rangle_{\rm dis} - |\ln(\omega/a_0)|^{-2}$ computed numerically. The disorder strength is set $W = 1$. The constant $a_0 \simeq 0.8$ is determined to minimize the errors e_i. It can be seen that $e_1(\omega) \propto \omega$ and $e_2(\omega) \propto \omega^2$.

with coinciding spatial arguments is obtained from the ground state of the corresponding effective Schrödinger equation. We obtain, in agreement with Ref. [36],

$$\langle G(i\omega)\rangle_{\rm dis} = \frac{a_1 W}{i\omega|\ln(\omega/a_0 W)|^2}. \tag{D1}$$

We have found the constants a_1 and a_0 by a numerical solution of the effective Schrödinger equation of the supersymmetric quantum mechanics; the results are $a_1 = 1$ (which holds with a very high accuracy and is apparently exact) and $a_0 \simeq 0.8$. Extending this analysis to the averaged square of the Green's function, we obtain

$$\langle G(i\omega)G(i\omega)\rangle_{\rm dis} = \frac{a_2 W}{\omega^2|\ln(\omega/a_0 W)|^2}, \tag{D2}$$

where $a_2 = 1/3$ (which again holds numerically with a very high accuracy and should thus be exact). Equations (D1) and (D2) are derived in the continuum-limit approximation to the effective Schrödinger equation. We have verified, however, by a numerical solution of the exact (discrete) equation that they hold with an outstanding accuracy. Specifically, as shown in Fig. 30, the relative correction to Eq. (D1) is of the order ω and that to Eq. (D2) is of the order ω^2. This means, in particular, that all orders of expansion of Eqs. (D1) and (D2) in $1/|\ln\omega|$ are fully reliable.

Now we connect these results to the correlation functions of eigenstates $\psi_\alpha(r)$ (which are continuum limit counterparts of the states $U_{i\alpha}$ studied numerically in Sec. V. Since all arguments of Green's functions that we consider are equal (we set them $r = 0$), only eigenstates at this point will enter. Using the spectral decomposition of the single-particle Green's function, we get

$$\langle G(i\omega)\rangle_{\rm dis} = \sum_\alpha \left\langle \frac{\psi_\alpha^2(0)}{i\omega - \epsilon_\alpha}\right\rangle_{\rm dis} = \int d\epsilon\, L\, \nu(\epsilon)\frac{\langle\psi_\alpha^2(0)\rangle_{\rm dis}}{i\omega - \epsilon}. \tag{D3}$$

The average entering here is $\langle\psi_\alpha^2(0)\rangle_{\rm dis} = L^{-1}$ due to eigenfunction normalization. Further, the density of states is

$$\nu(\epsilon) \simeq \frac{c^2}{\epsilon|\ln(\epsilon/\Lambda)|^3}, \tag{D4}$$

see Eq. (34), where $c \sim 1$ is the constant defined in Eq. (36) and we have introduced the ultraviolet cutoff $\Lambda \sim 1$. Substituting this in Eq. (D3), we get

$$\langle G(i\omega)\rangle_{\rm dis} = c^2\left[\frac{1}{i\omega|\ln\omega/\Lambda|^2} + \frac{\ln 2}{i\omega|\ln\omega/\Lambda|^3} + \mathcal{O}(\omega^{-1}|\ln\omega|^{-4})\right]. \tag{D5}$$

We see that Eq. (D5) is in full agreement with the result (D1) of the supersymmetric calculation. Indeed, not only the leading behavior agrees but also Eq. (D1) can be expanded to bring it to the form (D5). This confirms that the formula (D4) for the density of states that we have used when deriving Eq. (D5) from the spectral decomposition (D3) is correct. One can, of course, also obtain (D4) by performing an analytical continuation of Eq. (D1). Note, however, that we used different models of disorder in the numerical and analytical calculations, so that numerical value of the coefficient c^2 in Eq. (D4) cannot be directly obtained from the analytical result.

Having satisfied ourselves that the spectral decomposition works properly for $\langle G(i\omega)\rangle_{\rm dis}$, we turn to $\langle G(i\omega)G(i\omega)\rangle_{\rm dis}$ that provides information about correlations of different eigenfunctions. The spectral decomposition now yields

$$\langle G(i\omega)G(i\omega)\rangle_{\rm dis} = \sum_\alpha \left\langle \frac{\psi_\alpha^4(0)}{(\epsilon_\alpha - i\omega)^2}\right\rangle_{\rm dis} + \sum_{\alpha\neq\beta}\left\langle \frac{\psi_\alpha^2(0)\psi_\beta^2(0)}{(\epsilon_\alpha - i\omega)(\epsilon_\beta - i\omega)}\right\rangle_{\rm dis}. \tag{D6}$$

In Sec. V, we have found numerically the following scaling of the eigenstates correlation functions entering Eq. (D6): $\langle\psi_\alpha^4(0)\rangle_{\rm dis} = aL^{-1}$, Eq. (53), and $\langle\psi_\alpha^2(0)\psi_\beta^2(0)\rangle_{\rm dis} = bL^{-2}\ln\epsilon_>$, Eq. (56), where a and b are numerical coefficients, and $\epsilon_>$ is the larger of the two energies ϵ_α and ϵ_β. Substituting them into Eq. (D6) and rewriting the sum over energies as integrals with the density of states (D4), we obtain

$$\langle G(i\omega)G(i\omega)\rangle_{\rm dis} = c^2\left[\frac{a}{i\omega^2|\ln\omega/\Lambda|^2} + \frac{a - (2/3)bc^2}{i\omega^2|\ln\omega/\Lambda|^3} + \mathcal{O}(\omega^{-1}|\ln\omega|^{-4})\right]. \tag{D7}$$

We observe now that two leading terms of Eq. (D7) fully correspond to the expansion of the result (D2) of the supersymmetry-formalism calculation. This proves that the numerically found values of the exponents, $\alpha = 1$ and $\gamma = 2$, in the scaling of eigenstate correlations, Eq. (56), are indeed exact.

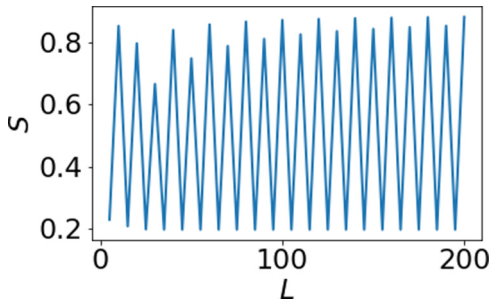

FIG. 31. Entanglement entropy S of the central bond vs system size L of the interacting Majorana chain with staggering, Eq. (17). The parameters $t^{(1)} = 1.00$, $t^{(2)} = 0.72$, $g^{(1)} = 1.5$, and $g^{(2)} = 1.08$ are chosen in such a way that the system belong to the red region in Fig. 3. Apart from even-odd oscillations, the entanglement entropy stays constant with system size. Thus the system is gapped for these parameters.

APPENDIX E: ENTANGLEMENT ENTROPY IN GAPPED REGIME OF THE MAJORANA CHAIN WITH REPULSIVE INTERACTION AND STAGGERING

In the phase diagram of the clean interacting Majorana chain with staggering (Fig. 3), we observe a region (plotted in red) where application of formula (18) yields a very high apparent central charge. This is in contrast to the dual region (obtained by reflection with respect to the self-dual line) where the formula yields a central charge of zero consistent with the expectation of a gapped phase. Thus the region above the critical line should be gapped as well. To check this, we have calculated the entanglement entropy S at the central bond for different system sizes. The result shown in Fig. 31 unambiguously exhibits the area law for S (i.e., no increase with L), so that the region is gapped. This is not in contradiction with the high apparent central charge observed in Fig. 3, since the formula (18) is guaranteed to be valid only in conformal theories. On the other hand, in other gapped regions the entanglement entropy did not show any anomalies of this type. It is thus interesting to look more closely at this region in order to understand the reasons for the anomalous behavior of S there.

To shed light on the behavior of the entanglement entropy, we compare in Fig. 32 the σ^x correlator with the entanglement entropy as function of bond position. The entanglement entropy increases sharply around the central bond leading to a spurious high value of the central charge if it is calculated by formula Eq. (18). The correlator $\langle \sigma^x_{L/4}\sigma^x_{L/4+i}\rangle$ shows two regions of antiferromagnetic order with a phase shift at $i = L/2$.

Considering points in the phase diagram of Fig. 3 in a narrow region between the red patch and the extended critical region with $c = 1$. Here the σ^x correlator looks very similar, except that there is more then one node where the phase of the antiferromagnetic ordering shifts. A characteristic example is shown in the left panel of Fig. 33. By comparing this plot with the entanglement entropy of the same system (right panel of Fig. 33), we see that each of these nodes is associated with a maximum in the entanglement entropy. We find that the number of such nodes depends on parameters of the

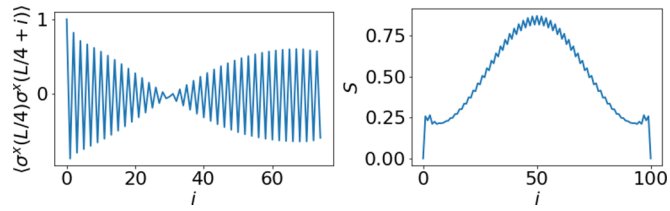

FIG. 32. Spin-spin correlator $\langle\sigma^x(L/4)\sigma^x(L/4+i)\rangle$ vs distance i(left) and entanglement entropy at the bond i (right) of a system with Hamiltonian (17) and parameters $t^{(1)} = 1.00$, $t^{(2)} = 0.72$, $g^{(1)} = 1.5$, $g^{(2)} = 1.08$, and $L = 100$. These parameters belong to the red region in Fig. 3. The σ^x spin component shows the antiferromagnetic order but the π phase shifts occurs at the central bond. In view of this, the spin correlator in the left panel takes there a zero value. The entanglement entropy in the right panel has a peak around the same spatial point.

Hamiltonian and on the system size. Furthermore, it also depends on whether the system size is even or odd. This explains the difference between even and odd system sizes in Fig. 31. We leave a more detailed analysis of the physics in this regime to future work.

We have verified that the peculiarity of this type does not arise in other regions of the phase diagram in Fig. 3. In those regions, the central charge obtained by fitting the x dependence of the entanglement entropy $\mathcal{S}$ at fixed L according to Eq. (18) is consistent with that found from the L dependence of $\mathcal{S}$.

APPENDIX F: CORRELATION FUNCTIONS AWAY FROM CRITICALITY

In Sec. V B 2, we studied Hartree, Fock, and Hartree-Fock correlations of two eigenfunctions. We focused there on the critical regime of sufficiently small r, which is of particular physical interest and also the one needed to describe the effect of a finite-range interaction. For completeness, we discuss here the range of large r, such that the system is away from criticality. The scaling (56) of the correlation function C_H is expected to hold as long as the system is at criticality, i.e., at $r < \xi_\epsilon$. (The same applies to C_F, which is nearly equal

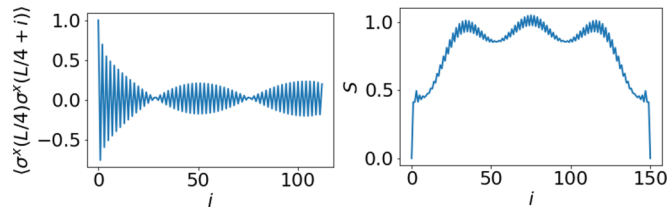

FIG. 33. Spin-spin correlator $\langle\sigma^x(L/4)\sigma^x(L/4+i)\rangle$ vs distance i(left) and entanglement entropy at bond i (right) of a system with Hamiltonian (17) and parameters $t^{(1)} = 1.00$, $t^{(2)} = 0.90$, $g^{(1)} = 1.5$, $g^{(2)} = 1.35$, and $L = 150$. In the indices, $L/4$ denotes the integer part $[150/4] = 37$. In the phase diagram of Fig. 3, these parameters put the system just below the red patch, but still outside the LL region. For these parameters and length, the antiferromagnetic ordering of the σ^x spin component changes phase several times, as seen in the left panel. The entanglement entropy in the right panel exhibit peaks at the corresponding bonds.

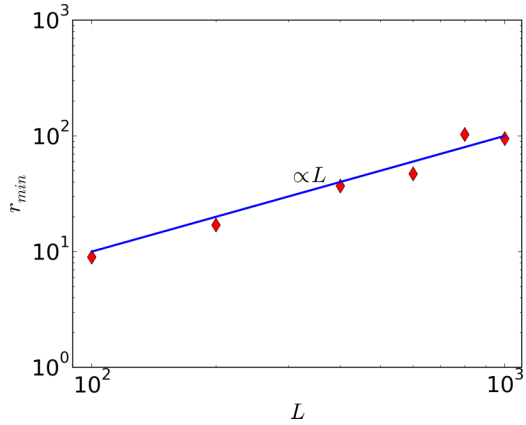

FIG. 34. Numerically found position $r_{\min}$ of the minimum of $C_H(\epsilon_1, \epsilon_2, r, L)$ with respect to r, as a function of length L. This minimum determines the upper border of the critical regime, see left panel of Fig. 19. The scaling $r_{\min} \propto L$ is found, confirming the expectation that the critical regime extends up to ξ_ϵ with $\epsilon = \epsilon_2$.

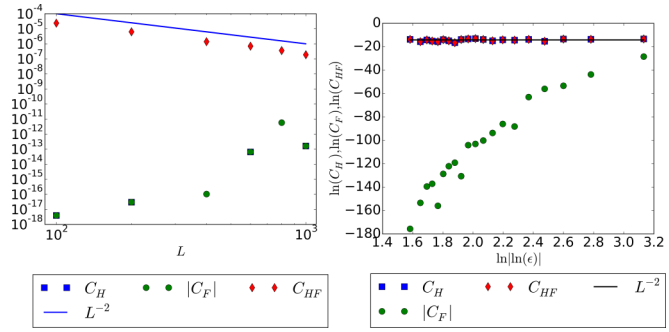

FIG. 35. Correlation at large distances. (Left) matrix elements $C_H(\epsilon_1, \epsilon_{20}, r = 150, L)$, $C_F(\epsilon_1, \epsilon_{20}, r = 150, L)$, and $C_{\rm HF}(\epsilon_1, \epsilon_{20}, r = 150, L)$ as functions of the system size L. (Right) $C_H(\epsilon_1, \epsilon, r = 1000, L = 1200)$, $C_F(\epsilon_1, \epsilon, r = 1000, L = 1200)$, and $C_{\rm HF}(\epsilon_1, \epsilon, r = 1000, L = 1200)$ as functions of energy ϵ. In both panels, C_H shows the behavior (F1) corresponding to the loss of correlations. The Fock correlation functions is much smaller in this regime, $C_F \ll C_H$.

to C_H in the critical regime.) According to Eqs. (54) and (36), the localization length ξ_ϵ is equal to the system size L times some numerical coefficient, if we choose the second level ϵ_2 as the larger of two energies, as is done, e.g., in the left panel of Fig. 19. In this figure, $L = 400$ and the critical regime extends up to $L \simeq 20$. In order to check that the upper border of the critical regime is indeed equal to L times a numerical coefficient, we plot in Fig. 34 the position $r_{\min}$ of the minimum of $C_H(\epsilon_1, \epsilon_2, r, L)$ with respect to r, as a function of L. As is clear from the left panel of Fig. 19, this minimum essentially marks the upper border (with respect to r) of the critical regime, which is expected to be $\sim \xi_\epsilon$. We see that the expectation that $r_{\min}$ scales as L is confirmed, i.e., the critical regime extends up to ξ_ϵ, as expected.

Now we turn to the behavior of the correlation functions for $r > \xi_\epsilon$, i.e., outside of the critical regime. For separation $r \sim L$, the states are expected to lose all correlations, which implies that

$$C_H(\epsilon, r \sim L, L) \sim \frac{1}{L^2}. \tag{F1}$$

The saturation of the correlation function C_H at a value $\sim 1/L^2$ at large r is evident in the left panel of Fig. 19. As a further check, we show in Fig. 35 the L dependence (left panel) and ϵ dependence (right panel) of C_H for $r \sim L$. The figure confirms that, in this regime, $C_H \sim L^{-2}$ and is essentially ϵ-independent.

It is interesting to notice that the critical behavior (56) at its upper border $r \sim \xi_\epsilon \sim \ln^2 \epsilon$ yields $C_H \sim 1/L^2 \ln^2 \epsilon$, which does not match Eq. (F1) due to an additional factor $1/\ln^2 \epsilon \ll 1$. Thus there should be an intermediate regime for $\xi_\epsilon < r < L$ located between the critical regime (56) and the uncorrelated regime (F1). This regime, where C_H rapidly increases with r, is clearly observed in the left panel of Fig. 19. We leave an analysis of this regime to a future work.

Finally, we note that for large distances $r > \xi_\epsilon$ (i.e., outside of the critical regime), the Fock term becomes much smaller than the Hartree one, $C_H \gg C_F$, see Figs. 19 and 35. Therefore the strong Hartree-Fock cancellation (which occurs for even r) is only a property of the critical regime. Another interesting observation is that the Fock term changes sign around $r \sim \xi_\epsilon$. This explains the dips in the curves for $|C_F|$, see Figs. 19 and 25.

[1] F. D. M. Haldane, Rev. Mod. Phys. **89**, 040502 (2017).
[2] K. Nomura, M. Koshino, and S. Ryu, Phys. Rev. Lett. **99**, 146806 (2007).
[3] J. E. Moore, Nature (London) **464**, 194 (2010).
[4] P. M. Ostrovsky, I. V. Gornyi, and A. D. Mirlin, Phys. Rev. Lett. **98**, 256801 (2007).
[5] S. Ryu, C. Mudry, H. Obuse, and A. Furusaki, Phys. Rev. Lett. **99**, 116601 (2007).
[6] S. D. Sarma, M. Freedman, and C. Nayak, npj Quantum Inf. **1**, 15001 (2015).
[7] J. Alicea, Rep. Prog. Phys. **75**, 076501 (2012).
[8] M. Leijnse and K. Flensberg, Semicond. Sci. Technol. **27**, 124003 (2012).
[9] C. Beenakker, Annu. Rev. Condens. Matter Phys. **4**, 113 (2013).
[10] A. Altland and R. Merkt, Nucl. Phys. B **607**, 511 (2001).
[11] A. Kitaev, AIP Conf. Proc. **1134**, 22 (2009).
[12] A. P. Schnyder, S. Ryu, A. Furusaki, and A. W. W. Ludwig, Phys. Rev. B **78**, 195125 (2008).
[13] S. Ryu, A. P. Schnyder, A. Furusaki, and A. W. W. Ludwig, New J. Phys. **12**, 065010 (2010).
[14] A. D. Mirlin, F. Evers, I. V. Gornyi, and P. M. Ostrovsky, Int. J. Mod. Phys. B **24**, 1577 (2010).
[15] L. Fu and C. L. Kane, Phys. Rev. B **76**, 045302 (2007).

[16] L. Fu, Phys. Rev. Lett. **106**, 106802 (2011).
[17] L. Fidkowski and A. Kitaev, Phys. Rev. B **83**, 075103 (2011).
[18] L. Fidkowski and A. Kitaev, Phys. Rev. B **81**, 134509 (2010).
[19] T. Morimoto, A. Furusaki, and C. Mudry, Phys. Rev. B **92**, 125104 (2015).
[20] M. S. Foster and E. A. Yuzbashyan, Phys. Rev. Lett. **109**, 246801 (2012).
[21] M. S. Foster, H.-Y. Xie, and Y.-Z. Chou, Phys. Rev. B **89**, 155140 (2014).
[22] P. M. Ostrovsky, I. V. Gornyi, and A. D. Mirlin, Phys. Rev. Lett. **105**, 036803 (2010).
[23] I. S. Burmistrov, I. V. Gornyi, and A. D. Mirlin, Phys. Rev. Lett. **108**, 017002 (2012).
[24] A. M. Finkel'stein, Int. J. Mod. Phys. B **24**, 1855 (2010).
[25] A. Kitaev, Phys. Usp. **44**, 131 (2001).
[26] A. Rahmani, X. Zhu, M. Franz, and I. Affleck, Phys. Rev. B **92**, 235123 (2015).
[27] C.-K. Chiu, D. I. Pikulin, and M. Franz, Phys. Rev. B **91**, 165402 (2015).
[28] D. I. Pikulin, C.-K. Chiu, X. Zhu, and M. Franz, Phys. Rev. B **92**, 075438 (2015).
[29] C.-K. Chiu, D. I. Pikulin, and M. Franz, Phys. Rev. B **92**, 241115(R) (2015).
[30] V. Shivamoggi, G. Refael, and J. E. Moore, Phys. Rev. B **82**, 041405(R) (2010).
[31] V. Mourik, K. Zuo, S. M. Frolov, S. R. Plissard, E. P. A. M. Bakkers, and L. P. Kouwenhoven, Science **336**, 1003 (2012).
[32] A. Milsted, L. Seabra, I. C. Fulga, C. W. J. Beenakker, and E. Cobanera, Phys. Rev. B **92**, 085139 (2015).
[33] S. Nadj-Perge, I. K. Drozdov, J. Li, H. Chen, S. Jeon, J. Seo, A. H. MacDonald, B. A. Bernevig, and A. Yazdani, Science **346**, 602 (2014).
[34] A. Bühler, N. Lang, C. V. Kraus, G. Möller, S. D. Huber, and H. P. Büchler, Nat. Commun. **5**, 4504 (2014).
[35] D. S. Fisher, Phys. Rev. B **50**, 3799 (1994).
[36] L. Balents and M. P. A. Fisher, Phys. Rev. B **56**, 12970 (1997).
[37] D. S. Fisher, Phys. Rev. B **51**, 6411 (1995).
[38] S. R. White, Phys. Rev. B **48**, 10345 (1993).
[39] D. Jaschke, M. L. Wall, and L. D. Carr, Comput. Phys. Commun. **225**, 59 (2018).
[40] C.-K. Chiu, J. C. Y. Teo, A. P. Schnyder, and S. Ryu, Rev. Mod. Phys. **88**, 035005 (2016).
[41] A. Luther and I. Peschel, Phys. Rev. B **12**, 3908 (1975).
[42] G. Refael and J. E. Moore, Phys. Rev. Lett. **93**, 260602 (2004).
[43] G. Refael and J. E. Moore, J. Phys. A: Math. Theor. **42**, 504010 (2009).
[44] N. Laflorencie, Phys. Rev. B **72**, 140408(R) (2005).
[45] R. Kennedy and M. R. Zirnbauer, Commun. Math. Phys. **342**, 909 (2016).
[46] U. Schollwoeck, Annals of Physics **326**, 96 (2011).
[47] A. Bazavov, Y. Meurice, S.-W. Tsai, J. Unmuth-Yockey, L.-P. Yang, and J. Zhang, Phys. Rev. D **96**, 034514 (2017).
[48] P. Sen and B. K. Chakrabarti, Phys. Rev. B **43**, 13559 (1991).
[49] N. M. Gergs, L. Fritz, and D. Schuricht, Phys. Rev. B **93**, 075129 (2016).
[50] M. McGinley, J. Knolle, and A. Nunnenkamp, Phys. Rev. B **96**, 241113(R) (2017).
[51] T. Giamarchi and H. J. Schulz, Phys. Rev. B **37**, 325 (1988).
[52] I. S. Burmistrov, I. V. Gornyi, and A. D. Mirlin, Phys. Rev. B **92**, 014506 (2015).
[53] D.-H. Lee and Z. Wang, Phys. Rev. Lett. **76**, 4014 (1996).
[54] Z. Wang, M. P. A. Fisher, S. M. Girvin, and J. T. Chalker, Phys. Rev. B **61**, 8326 (2000).
[55] I. S. Burmistrov, S. Bera, F. Evers, I. V. Gornyi, and A. D. Mirlin, Ann. Phys. **326**, 1457 (2011).
[56] F. Evers and A. D. Mirlin, Rev. Mod. Phys. **80**, 1355 (2008).
[57] I. A. Gruzberg, A. D. Mirlin, and M. R. Zirnbauer, Phys. Rev. B **87**, 125144 (2013).
[58] F. J. Dyson, Phys. Rev. **92**, 1331 (1953).
[59] R. H. McKenzie, Phys. Rev. Lett. **77**, 4804 (1996).
[60] M. Titov, P. W. Brouwer, A. Furusaki, and C. Mudry, Phys. Rev. B **63**, 235318 (2001).
[61] M. S. Foster (unpublished).
[62] S. Bravyi and R. König, Commun. Math. Phys. **316**, 641 (2012).
[63] A. Rahmani, D. Pikulin, and I. Affleck, Phys. Rev. B **99**, 085110 (2019).
[64] I. V. Gornyi, A. D. Mirlin, and D. G. Polyakov, Phys. Rev. Lett. **95**, 206603 (2005).
[65] A. Pal and D. A. Huse, Phys. Rev. B **82**, 174411 (2010).
[66] R. Nandkishore and D. A. Huse, Annu. Rev. Condens. Matter Phys. **6**, 15 (2015).
[67] D. A. Abanin, E. Altman, I. Bloch, and M. Serbyn, Rev. Mod. Phys. **91**, 021001 (2019).
[68] I. A. Gruzberg, N. Read, and S. Vishveshwara, Phys. Rev. B **71**, 245124 (2005).
[69] K. S. Tikhonov and A. D. Mirlin, Phys. Rev. B **99**, 024202 (2019).
[70] S. Sachdev and J. Ye, Phys. Rev. Lett. **70**, 3339 (1993).
[71] A. Altland, D. Bagrets, and A. Kamenev, arXiv:1908.11351.
[72] A. Altland, D. Bagrets, and A. Kamenev, Phys. Rev. Lett. **123**, 106601 (2019).
[73] A. Altland, D. Bagrets, L. Fritz, A. Kamenev, and H. Schmiedt, Phys. Rev. Lett. **112**, 206602 (2014).
[74] A. Altland, D. Bagrets, and A. Kamenev, Phys. Rev. B **91**, 085429 (2015).